

A comprehensive multiphonon spectral analysis in MoS₂

Tsachi Livneh^{1*#} and Jonathan E. Spanier²

¹ *Department of Physics, Nuclear Research Center, Negev, P.O. Box 9001, Beer-Sheva, 84190, Israel.*

² *Department of Materials Science & Engineering, and Department of Physics, Drexel University, 3141 Chestnut St., Philadelphia, PA, 19104, USA.*

ABSTRACT

We present a comprehensive multiphonon Raman and complementary infrared analysis for bulk and monolayer MoS₂. For the bulk the analysis consists of symmetry assignment from which we obtain a broad set of allowed second-order transitions at the high symmetry M, K and Γ Brillouin zone (BZ) points. The attribution of about 80 transitions of up to fifth order processes are proposed in the low temperature (95 K) resonant Raman spectrum measured with excitation energy of 1.96 eV, which is slightly shifted in energy from the *A* exciton. We propose that the main contributions come from four phonons: A_{1g} (M), E¹_{2g} (M₂), E²_{2g} (M₁) (TA' (M)) and E²_{2g} (M₂) (LA' (M)). The last three are single degenerate phonons at M with an origin of the E¹_{2g} (Γ) and E²_{2g} (Γ) phonons. Among the four phonons, we identify in the resonant Raman spectra all (but one) of the second-order overtones, combination and difference-bands and many of the third order bands. Consistent with the expectation that at the M point only combinations with the same inversion symmetry (*g* or *u*) are Raman-allowed, the contribution of combinations with the LA(M) mode can not be considered with the above four phonons. Although minor, contributions from K point and possibly Γ -point phonons are also evident.

The '2LA band', measured at ~ 460 cm⁻¹ is reassigned. Supported by the striking similarity between this band, measured under off-resonant conditions, and recently published two phonon density of states, we propose that the lower part of the band, previously attributed to 2LA(M), is due to a van Hove singularity between K and M. The higher part, previously attributed exclusively to the A_{2u} (Γ) phonon, is mostly due to the LA and LA' phonons at M.

For the monolayer MoS₂ the second-order phonon processes from the M and Γ Brillouin zone points are also analyzed and are discussed within similar framework to that of the bulk.

1. Introduction

Recently, Raman scattering has been increasingly important in the study of transition-metal-layered-type-dichalcogenides [1-16]. Among those, the most investigated system is the indirect semiconductor MoS₂, with the *2H* hexagonal polytype (D_{6h}⁴ space group #194), which becomes a direct band-gap semiconductor in monolayer *1H* polytype [16]. Raman scattering was employed for the various forms of bulk [1-6], Inorganic Fullerenes (IF) [7] and few layer (FL) structures down to the monolayer [8-13]. A group-theoretical analysis of the optical lattice vibrations for the bulk [1] reveals four Raman-active modes corresponding to the following symmetries with measured frequencies under ambient conditions: E_{2g}² (35 cm⁻¹), E_{1g} (286 cm⁻¹), E_{2g}¹ (383 cm⁻¹), and A_{1g} (408 cm⁻¹). In addition, there are two IR-active modes: E_{1u} (384 cm⁻¹), A_{2u} (470 cm⁻¹), and four silent modes: B_{2g}² (58 cm⁻¹) [11], E_{2u} (287 cm⁻¹), B_{1u} (403 cm⁻¹) and B_{2g}¹ (~ 475 cm⁻¹). In addition to observation of first-order Raman lines these and other studies showed a rich multiphonon spectrum [2, 3, 6, 7, 9, 10, 13-15] with sensitivity to excitation energy [6, 7, 9, 10, 13].

The higher order spectra of bulk MoS₂ have been assigned [2, 3] to be mostly constructed from second-order transitions (some of which include the longitudinal acoustic (LA) phonon at the M Brillouin zone (BZ) edge, LA(M), and BZ center Γ -point phonons). Stacy and Hodul [3] focused on the nature of the band around ~ 460 cm⁻¹, which is denoted hereafter as the ‘2LA band’ and assigned it to a second-order process involving the LA(M) phonon. Frey *et al.* [7] studied this band for inorganic fullerenes (IF) and bulk MoS₂, suggesting that the asymmetric features of 2LA band are due to a combination of two peaks centered at room temperature at ~454 cm⁻¹ (denoted here as α_1) and ~ 465 cm⁻¹ (α_2). The first is assigned to the 2LA(M) and the second to a Raman-forbidden IR-allowed optical A_{2u}(Γ) mode, which involves asymmetric translation of both Mo and S atoms parallel to the *c* axis [1]. It was argued that, although not allowed by Raman selection rules, under resonance conditions excitons could mediate the scattering of this phonon. The above assignment of the ‘2LA band’ has been adopted exclusively in the literature [6-15].

Although the K-point phonons may also contribute, it was proposed that due to the fact that the 2LA(K) frequency was found (according to Ref. 17) to be higher by ~10 cm⁻¹ at the K point relative to the M point, their contribution is minor. This was in contrast to *2H*-WS₂, which was argued by Sourisseau *et al.* [17] to have a multiphonon spectrum mostly constructed from combination and difference bands with LA phonons at the K point.

Here we present a comprehensive multiphonon analysis in bulk *2H*-MoS₂. Supported by new evidence, we propose modified interpretations and assignments of some of the central spectral

features. Significantly, our findings challenge the widely accepted one [3] according to which the majority of the observed second-order combination and difference bands from the M point are due to one of the $A_{1g}(M)$, and to what is referred to as $E_{1g}(M)$ and $E_{2g}(M)$ phonons with LA(M) phonons, or as recently proposed by Golasa *et al.* [14, 15], with transverse acoustic (TA(M)) and/or out-of-plane transverse acoustic (ZA(M)) phonons. We complement our analysis by exploring the multiphonon spectrum of monolayer *1H*-MoS₂ (while leaving FL systems for later study) and anticipate that our full study will significantly advance fundamental understanding of the origin of multiphonon resonant inelastic light scattering processes in layered dichalcogenides and their application.

2. Experiment

Resonant Raman spectra for a bulk sample were measured in backscattering configuration using a Jobin-Yvon LabRam HR spectrometer with a He-Ne 632.8 nm laser (1.96 eV), which is slightly shifted in energy from the *A* exciton [18]. The scattered light was dispersed by a 1800 grooves/mm grating resulting in a $<1 \text{ cm}^{-1}$ spectral resolution. The low temperature spectra were measured at 95 K by means of a Linkam model THMS600 continuously - cooled liquid-nitrogen stage. UV-Raman was measured with He-Cd 325 nm laser (3.81 eV).

Off-resonant Raman spectra for bulk MoS₂ were also measured in the backscattering configuration using a Renishaw spectrometer with a 785 nm (1.58 eV) and a 514.5 nm (2.41 eV) lasers. Raman spectra measured at 1064 nm (1.16 eV) were acquired by using Bruker FT-Raman spectrometer. Raman spectra from a monolayer of MoS₂ were measured at 632.8 nm (1.96 eV). The power of the laser was kept sufficiently low to avoid heating effects.

Single and few-layer MoS₂ films were isolated from bulk MoS₂ crystals by mechanical exfoliation method and placed on a silicon substrate covered by a thick SiO₂ layer. After confirming that the distinctive Stokes Raman spectrum of the monolayer was consistent with previously published spectra [9], the monolayer thickness was verified by topographic-height scanning probe microscopy (Asylum Research MFP-3D).

3. Results and discussions

A. Symmetry mode analysis of multiphonon bulk $2H\text{-MoS}_2$

In hexagonal MoS_2 there are six atoms in the unit cell and therefore 18 branches of the phonon dispersion relation, some of which are degenerate in high symmetry directions [19]. **Table 1** presents a list of phonons in $2H\text{-MoS}_2$ with their symmetry assignments, divided into the phonons symmetries at Γ (Brillouin zone-center) and at M and K (zone-edge points in the $(\xi 0 0)$ and $(\xi \xi 0)$ directions in \mathbf{k} space, respectively). For the D_{6h}^4 space group the eigenstates at M and K points correspond to irreducible representations of the point groups D_{2h} and D_{3h} , respectively. In Table 1 we also show the frequencies of the various phonons. For the Γ point we show experimentally measured frequencies at 300 K. For the M and K points the listed frequencies are the proposed values that are expected at low temperatures, in accordance with DFT calculations (and will be used to assign the resonant Raman spectrum at 95 K as described in Section B). We followed Sourisseau *et al.* [17] in assigning the symmetry of the M point BZ phonons, while consulting the correlation tables between the point group of D_{6h} and its subgroups [20]. In labeling the symmetry of the representations we use the Mulliken notation [21]. Major aspects of constructing Table 1 are discussed in the supporting information.

Each phonon branch is denoted with a letter (capital for Γ , Greek alphabet for M and regular for K). The phonon notation $E_{1g}(M_1)$, for example, denotes one of a doubly degenerate phonon at Γ of E_{1g} symmetry, which splits and extends to M, where it has symmetry belonging to the D_{2h} point group. We note that due to this splitting there are two different phonons at M (M_1 and M_2). Hence, the extensively used notation [3, 15, 16] of phonons at M that originate from doubly degenerate phonons at Γ (like $E_{1g}(M)$ and $E_{2g}^1(M)$) is not suitable. In Table 1 we also distinguish acoustic phonons as LA, TA or ZA and we denote the phonons at M originating as quasi-acoustic optical $B_{2g}^2(\Gamma)$ and $E_{2g}^2(\Gamma)$ phonons as $ZA'(B_{2g}^2(M))$ and $TA'(E_{2g}^2(M_1))+LA'(E_{2g}^2(M_2))$, respectively. The LA' and TA' phonons will be argued to be central in the multiphonon resonant process.

At the K point all the phonons are assigned as singly degenerate, excluding two doubly degenerate modes which originate from $E_{1g}(M_1)+E_{2u}(M_2)$ and $E_{2g}^1(M_1)+E_{1u}^1(M_2)$ (see supporting information).

Key in the analysis is the correlation of experiments with symmetry-based prediction of multiphonon transitions. Observation of high-order multiphonon processes demands accurate predictions. There are few published DFT calculations [22- 24] that present the various phonon dispersions in $2H\text{-MoS}_2$. We extracted from those the calculated frequencies of the various M and K-point phonons. Correlating experiment with calculation, particularly for the M-point phonons, and noting that DFT estimates are for 0 K and will have at best a few % error in calculated mode energies, we introduce a tolerance of up to $\pm 10 \text{ cm}^{-1}$ around the low temperatures measured value to facilitate the analysis. This is due to our ability to ‘fine tune’ those frequencies by carefully looking at the resonant multiphonon bands, as shown below. Since some of the frequencies participate in several transitions involving high-order processes there is high sensitivity to our changes. Therefore the frequencies that we show in Table 1 are proposed and should be considered as such. Indeed, the excellent fit between the predictions and the data for the M-point phonons indicates that those are very good predictions, particularly for the M point frequencies.

We next present a derivation of the symmetries of the Raman tensors of the second-order scattering from zone-edge phonons at M and K. We have listed in Table 1 the symmetries of the individual phonons at Γ , M and K points. We next determine the irreducible representations of the binary combinations at each of these points. For the Brillouin zone-center phonons with $\mathbf{k} = 0$ this is accomplished by simply multiplying together the characters of the individual group operations [25a]. The determination of transitions for $\mathbf{k} \neq 0$ phonons is less straightforward than that for $\mathbf{k} = 0$, particularly for cases of non-symmorphic space groups, which are having glide planes and screw axis, e.g., space group #194, D_{6h}^4 . Using the Bilbao crystallographic server [26] we obtained the Raman-active scattering tensors for second-order processes from phonons at M and K in the D_{6h}^4 space group and established the correlations between irreducible representations of the combinations of the group of a particular \mathbf{k} and the irreducible representations of the full space group. For a binary combination to be Raman-active at the M and K points it must correlate with at least one of the three Raman-active symmetries: A_{1g} , E_{2g} , and E_{1g} of point group D_{6h} . For a binary combination to be IR-active at the M and K points it must correlate with at least one of the two IR-active symmetries: A_{2u} and E_{1u} of point group D_{6h} . **Table 2** lists all the possible binary combinations for the M, K and Γ points and their Raman and IR activity for $2H\text{-MoS}_2$. Sets of scattering tensors of the Raman-active phonons are also shown [25b]. In order to construct them we reduced the products of binary combinations to their irreducible constituents and utilized the compatibility relations [26, 27] along $\Gamma \xrightarrow{\Sigma} M$, $\Gamma \xrightarrow{\Lambda} K$ and $M \xrightarrow{T} K$, as is briefly summarized in the supporting information.

All the modes in the M point (also for Γ) are either even or odd with respect to inversion (g or u , respectively). Hence, as is evidenced from Table 2 the transitions of M point are divided into either Raman or IR activity. For the K point most of the bands show activity on both. Furthermore, most of the M and K points second-order transitions that are active under parallel polarization backscattering configurations ($z(xx)\bar{z}$, $z(yy)\bar{z}$ in the Porto notation) are also active under perpendicular polarizations ($z(xy)\bar{z}$, $z(yx)\bar{z}$). We note that some of the transitions (with E_{1g} symmetry having $\alpha_{zx(xz)}$ and $\alpha_{yz(zy)}$ polarizability tensor components) are expected to be active under off-resonant conditions only under tilted configuration, for which $k \parallel c$ axis (although we do not exclude their activity under resonant conditions at non-tilted configuration). Hence, besides those transitions that are forbidden as a result of being odd with respect to inversion, all the second-order transitions are Raman allowed. A detailed discussion and analysis of the polarized Raman spectra, in accordance with our extensive analysis, will be given elsewhere.

According to our analysis some of the assignments for second-order transitions at the M point [3] that are currently cited in the literature are not symmetry-allowed. This is because they are combinations of modes with different inversion symmetries (g or u); below we show the assignment and their symmetry product: $A_{1g}(M)+LA(M)$ ($A_g \times B_{2u}$), $E^1_{2g}(M_2)+LA(M)$ ($A_g \times B_{2u}$), $E_{1g}(M_1)+LA(M)$ and $E_{1g}(M_2)+LA(M)$ ($B_{2g} \times B_{2u}$ and $B_{3g} \times B_{2u}$, respectively). In contrast, the symmetry products of the combinations that use instead the LA' phonon are symmetry allowed: $A_{1g}(M)+LA'(M)$ ($A_g \times A_g$), $E^1_{2g}(M_2)+LA'(M)$ ($A_g \times A_g$), $E_{1g}(M_1)+LA'(M)$ and $E_{1g}(M_2)+LA'(M)$ ($B_{2g} \times A_g$ and $B_{3g} \times A_g$, respectively). However, we bear in mind that an alternative symmetry-allowed ($B_{2u} \times B_{2u}$) combination with the LA(M) phonon ($E_{1u}(M_1)+LA(M)$) can be found at about similar frequency to that of the symmetry-forbidden combination of $E^1_{2g}(M_2)+LA(M)$. The same can also apply to some of the other combinations/difference bands (with $B_{1u}(M)$ phonons) that may potentially contribute at about similar frequencies to those of the $A_{1g}(M)$ phonons. In the resonant spectrum, which will be shown below and in our analysis henceforward, we consider the even-symmetry (with respect to inversion) second-order combinations/difference bands, which involve $A_{1g}(M)$ and $E^1_{2g}(M_2)$ (and not $B_{1u}(M)$ and $E^1_{1u}(M_1)$), the dominant ones. Our approach may be substantiated in further studies.

In accordance with the results of Tables 1 and 2, in **Tables 3** and **4** we present a complete set of frequencies of the $2H\text{-MoS}_2$ second-order Raman- and IR-active combinations, from phonons at M and K at low temperatures (Table 3) and for Γ at 300 K (Table 4). For the Raman-active bands the upper and lower numbers denote combination and difference bands, respectively. The

components for different active configurations (while maintaining the respective background colors which denote the various symmetries of Table 3) are also shown.

As mentioned above, unlike the case of the M point, most of the second-order combinations at the K point are both IR- and Raman-allowed. Additionally, the second-order bands that are constructed from *both* phonons of $A_{1g}(M)$, $E^1_{2g}(M_2)$, $E^2_{2g}(M_1)$ (TA' (M)) and $E^2_{2g}(M_2)$ (LA' (M)), which will be referred henceforward as the 'resonant group', are denoted in Table 3 with a thick blue frame (see supporting information for a comment on the nature of $E^1_{2g}(M_1)$). All those combinations are also characterized by temperature-dependent intensity (not shown), clearly indicating their resonant nature (with the A exciton). The focus on those bands allows us to narrow down the possibilities in analyzing the intricate resonant Raman spectrum, which contains about 80 transitions in the spectral range of 80-1130 cm^{-1} .

B. Resonant and off-resonant Raman scattering of bulk 2H-MoS₂

Shown in **Figure 1** is the Raman spectrum of 2H-MoS₂ at 95 K, measured using excitation energy of 1.96 eV in the spectral range of 80-850 cm^{-1} , and divided for clarity into four spectral sub-ranges (a-d). We also show positions of the second-order transitions' bands (active under the backscattering configuration with $\mathbf{k} \parallel c$ axis) of origin from M, K and Γ points, (Tables 3 and 4). For Γ , the estimated low-temperature frequencies were obtained from measured values at room temperatures [1-3] after adding of $\sim 2.5 \text{ cm}^{-1}$ (taking an estimated typical shift of $\sim 0.012 \text{ cm}^{-1}/\text{K}$ [5] for first-order phonons). For comparison the room temperature Raman spectrum using excitation energy of 1.58 eV is also shown (after being also shifted in frequencies towards those of lower temperatures for the sake of clarity). In order to highlight the second-order transitions at the M point that are due to the 'resonant group' the respective transitions are denoted by thicker blue marks. The rest of the M point group are denoted in red marks. It is clear from Figure 1 that the majority of the prominent bands are attributed to the 'resonant group' at M. However, some of the prominent bands cannot be attributed to this group and the contribution of 'off- resonant' M and from K and Γ -point phonons must be taken into account. An example is the band at $\sim 756 \text{ cm}^{-1}$. Shown in **Figure 2** is the off-resonant Raman scattering spectrum around this band, measured at 300 K, and $E_i = 1.58 \text{ eV}$. In order to facilitate the discrimination of the large number of potential spectral contributions we compare the Stokes and anti-Stokes spectra (frequency is shown in absolute scale). The calculated frequencies of second-order transitions at M, K and Γ are also shown with the denoted respective colors. Black arrows are pointing to the central frequencies of the contributing bands. Significantly,

some of the bands are masked in the Stokes spectrum and are ‘exposed’ in the corresponding anti-Stokes spectrum. The full spectral profile of the $\sim 756 \text{ cm}^{-1}$ band *cannot* be correlated exclusively with the M-point phonons. Clearly, some participation of K phonons and possibly Γ phonons is evident.

Finally, we emphasize that bands, which are very weak under resonant conditions, may become prominent in the spectrum, measured under off-resonant conditions. For example, the $E_{1g}(M_1)+E_{1g}(M_2)$ combination may be responsible for the band which appears at $\sim 632 \text{ cm}^{-1}$ in the low side of the $A_{1g}(M)+LA'(M)$ [9]. This band becomes visible as we move away from resonance with the A exciton, either by altering the excitation energy (on both sides of the $\sim 1.9 \text{ eV}$ resonance), or by increasing the temperature (as will be reported elsewhere).

Shown in **Figure 3** are sequences of all possible contributions (combination and difference bands) rendered in the form of ‘flowers’ for all the 2nd (circles) and 3rd (squares) order resonant transitions from the four ‘resonant group’ phonons. Processes that lead to negative shifts (like $LA'(M) - A_{1g}(M)$) are taken in their absolute values. At positions where neither is shown there is a process (e.g. $A_{1g}(M) + E_{2g}^2(M_1) - A_{1g}(M)$), which leads to first-order BZ-edge phonon scattering, and therefor not valid. Blue represents bands that are detected and red denotes bands not detected (possibly due to the low cross sections). Green represents a band that is possibly distinguishable or a band not found, but we believe may possibly be observed under adequate conditions. For example the $A_{1g}(M) - E_{2g}^1(M_2)$ that is expected at 42 cm^{-1} , below the filter cut-off. Furthermore, we expect this band to be strong, and examination of bulk spectra measured with $E_i = 1.96 \text{ eV}$ [28] reveals that it may be distinguishable. In fact, we anticipate that under resonance the following bands (and others that are not specified) may appear: 50 cm^{-1} ($E_{2g}^1(M_2)-2TA'(M)$), and 54 cm^{-1} ($2LA'(M)-A_{1g}(M)$). Some of the bands, marked in green, may be masked by other intense multiphonon bands.

The dominance of the ‘resonant group’ of phonons is expected particularly in the higher part of the spectrum where higher order transitions may be related exclusively with this group. Presented in **Fig. 4a** is a full set of up to 4th order contributions in the range of $830 - 1130 \text{ cm}^{-1}$ for $E_i = 1.96 \text{ eV}$ at 95 K. The denoted bands are constructed from up to 3rd order combinations of $E_{2g}^1(M_2)$ (ϕ_2) and $A_{1g}(M)$ (χ) phonons, subtracted or added to $TA'(M)$ (φ_1) or $LA'(M)$ (φ_2) phonons. In **Figure 4b** the Raman spectra at 300 K for $E_i = 1.96 \text{ eV}$ and $E_i = 1.58 \text{ eV}$ are compared. The intensities of the high-order bands decrease with an increase in temperature for $E_i = 1.96 \text{ eV}$ due to the departure from resonance [5], an observation that also affects lower-order multiphonon intensities [6]. In contrast, for $E_i = 1.58 \text{ eV}$ we find no spectral features beyond 825 cm^{-1} , which is consistent with the attribution of that spectral range to resonant multiphonon processes. Other bands (like $2B_{2g}^1(\Gamma)$ and

$2A_{2u}(\Gamma)$), which could potentially appear in this spectral range (see Table 4), evidently have null (or very minor) contribution.

It is clear from Fig. 3 that, excluding $A_{1g}(M)-E_{2g}^1(M_2)$, all the possible second-order combinations of single degenerate phonons at M with an origin at Γ of $A_{1g}(\Gamma)$, $E_{2g}^1(\Gamma)$ and $E_{2g}^2(\Gamma)$ phonons: $TA'(\varphi_1)$, $LA'(\varphi_2)$, $E_{2g}^1(M_2)(\phi_2)$, $A_{1g}(\chi)$ are observed in the resonant Raman spectra. In fact, many of the various third-order combinations are detected as well. Since the higher the scattering order the more quantitatively sensitive the spectral analysis, we further checked (beyond the presented spectrum in Fig. 4a) the consistency of the analysis by exploring the correlation between ‘expected’ and experimental band frequencies for a series of $nA+mB$ ($n=0-3$, $A=\chi, \phi_2$, $m=-1,0,1,2,3$, $B=\varphi_1, \varphi_2$). In **Figure 5** we plot $nA + mB$ vs. mB for various n . We compare the calculated (‘expected’) and measured frequencies. The correlation between the two is excellent, as is evident from the fact that most of the of 30 bands that are ‘expected’ (up to the 4th order) within the range of 100 - 1150 cm^{-1} are detected with small discrepancy of $\leq 3 \text{ cm}^{-1}$ between the calculated and measured values. Furthermore, higher order transitions are also detected in the room temperature spectrum, which was measured up to $\sim 1400 \text{ cm}^{-1}$ (see Fig. S1 presented in the supporting information).

In **Table 5** we list our proposed full assignments (most of which are resonant) of the up to 5th order multiphonon spectra (~ 80 transitions) measured up to $\sim 1130 \text{ cm}^{-1}$ at 95 K. It is important to note that additional bands, many of which are ‘masked’ by the intense resonant bands, are distinguishable under off-resonant conditions and warrant separate treatment guided by Tables 1-4, that were provided above. Assigning the full spectral range is a complicated task, due to the significant overlap between many of the multiphonon bands that may originate from the Γ , M and K points and to the need to take into account higher-order resonant transitions together with lower-order transitions that might be found in the same spectral position. The ability to be aided by temperature effects is, in some cases limited, under resonant conditions.

In Table 5 we firstly assign the 2nd order M-point bands of the above four phonons and of the ZA' (ι) phonon (see supporting information for a comment on the $E_{2g}^1(M_1)(\phi_1)$ phonon). The deviation between the measured frequencies and the ones shown in Table 3 is $\leq 3 \text{ cm}^{-1}$. Then we assign the resonant 3rd order process from the four phonons together with possible other 2nd order M-point processes and also 2nd order K and Γ -points phonons in accordance with Tables 1, 3 and 4. Finally, we assign the spectral range above 825 cm^{-1} (only observed under resonant conditions) with higher-order combinations constructed from M-point ‘resonant group’ phonons.

An important physical insight from this study, which presents a unified scenario consisting of symmetry analysis and quantitative band frequencies, is that the majority of resonant multiphonon combination processes is between M-point phonons that are from a branch that is optical at Γ . Furthermore, it seems that the cross sections for multiphonon bands that consist of A_{1g} (M) contribution tend to be higher (as can be deduced by the larger portion of detected bands of higher than second order). Although their existence is clear, the dominance of the K contributed transitions is low with respect to those from the M point

C. The nature of the Raman scattering ‘2LA band’

From the various bands the one denoted ‘2LA band’ is particularly interesting and following our analysis, this band now calls for reassignment. Previous resonance Raman studies on crystalline MoS₂ assigned this band to a second-order process involving the LA(M) phonon. The asymmetry of this peak was assigned to the inverse parabolic shape of the LA(M) dispersion curve near the M point in the BZ [3]. Frey *et al.* [7] suggested that the asymmetric features of the ~ 460 cm⁻¹ band is due to a combination of two peaks centered at room temperature at ~ 454 cm⁻¹ (denoted here as α_1) and ~ 465 cm⁻¹ (α_2). The first is assigned to the 2LA(M) and the second to a Raman-forbidden IR-allowed optical A_{2u} (Γ) mode, which involves asymmetric translation of both Mo and S atoms parallel to the c axis [1]. Unlike the α_2 band, which can be clearly assigned in Fig. 1, no feasible attribution to the α_1 band can be established (see the thick arrow in Fig. 1). Hence, there is a need to explore a different approach in order to trace its origin.

The phonon branches of bulk 2H-MoS₂ in the vicinity of M and K points, calculated by Acata *et al.* [22], are shown in **Figure 6a** with the respective extracted phonon density of states (PDOS). **Figure 6b** compares the spectra around ~ 460 cm⁻¹ for E_i from 1.16 eV to 3.81 eV. In addition, the 2PDOS profile (black line) [22] is also shown (after being shifted, for clarity, by a few cm⁻¹). The striking similarity between the ~ 460 cm⁻¹ band of all the spectra taken at E_i other than 1.96 eV and 3.81 eV, and the 2PDOS profile, suggests that the assignment of this band under off-resonant conditions is possibly attributed to combination of BZ edge phonons with additional features found in the PDOS.

In **Figure 6c** the (α_2/α_1) intensity ratio is depicted for the set of measurements after adding the respective ratios for 1.16, 1.58, 1.91 [13], 1.96, 2.09 [6] and 2.41 eV. The 2.09 eV measurement

is particularly important because it is expected to match exactly the B exciton incoming resonance at 300 K. It is evident that in the vicinity of the A exciton around ~ 1.9 eV the ratio increases dramatically. Based on temperature dependent measurements (not shown) which indicate a significantly stronger resonant dependence of α_2 than for α_1 , we conclude that there is a preferred resonance involving the A exciton for α_2 . This, in turn, explains why we see such a strong signal from this band only for ~ 1.9 eV excitation. The reason for the much stronger excitonic resonance of A with respect to that of B for the α_2 band needs further theoretical clarification.

The resonant nature and characteristics of the high energy side of the of the ~ 460 cm^{-1} band for the 3.81 eV spectra is fundamentally different from that of the 1.96 eV spectra. For the latter E_i , the α_2 band is constructed from second-order transitions at the M BZ point with no significant contribution of the $A_{2u}(\Gamma)$ mode. For the former E_i the main contribution, according to a recently published elaborate study of Lee *et al.* [30], comes from the $A_{2u}(\Gamma)$ mode at 470 cm^{-1} (bulk) and $A''_2(\Gamma)$ at ~ 465 cm^{-1} (monolayer), with the above mentioned ‘resonant group’ multiphonon contribution being very weak (Fig. S2 of Ref. 30). In fact, it is also shown that the $A_{2u}(\Gamma)$ mode is enhanced for $E_i=2.81$ eV. This may be attributed to a resonant excitation with a conduction band level, presumably positioned in the vicinity of the Γ BZ point [29], which, similar to the intensity of the $A_{2u}(\Gamma)$ band, seems to be particularly sensitive to the number of layers.

In **Figure 7** we show the Lorentzian line fit of the ~ 460 cm^{-1} band in the spectra taken at room temperature with $E_i = 1.96$ eV (bottom) and 1.58 eV (top). It is evident that this band is comprised of at least five contributions, denoted in the figure as L_1 - L_5 [31]. The α_1 band is comprised from L_1 and L_2 and α_2 from L_3 - L_5 . The distinction between those contributions is not only enhanced as we shift E_i with respect to the A exciton energy, but also as we depart from the resonance upon an increase in temperature. This can be seen in the inset of the lower part of Fig. 7 where we note the high similarity of the ‘2LA band’ spectrum taken at $E_i = 1.96$ eV and 573 K with the spectrum taken at room temperature and 1.58 eV. Both are off resonant in nature. Other than the red shift of the phonons under high temperatures, the spectral profiles are very similar.

For an appropriate assignment, it is important to realize that the M point is reached at ~ 230 cm^{-1} by two branches. The first is the $E^2_{1u}(M_1)$ acoustic branch that reaches the M point with B_{2u} symmetry phonon and the second is the $E^2_{2g}(M_2)$ branch that commences at Γ with the E^2_{2g} phonon and reaches M point with A_g symmetry [17]. We denote the former as LA and the latter as LA’, with

the former being estimated to be slightly ($\sim 2 \text{ cm}^{-1}$) higher than the latter, according to DFT calculations [23]. The two singly degenerate phonons reach the K point where they maintain their single degeneracy [24]. In line with the correlation with DOS we tentatively assign L_1 to a second-order band, possibly $A_{1g}(\Gamma)+E_{2g}^2(\Gamma)$, L_2 to a van Hove singularity between K and M (or actually contributions from singularities of two branches that fall at about the same frequency), L_3 and L_4 to the two phonons (LA' and LA, respectively) at M, and the weak L_5 band is tentatively assigned to the weak contributions of the two LA' and LA phonons at K with no significant contribution of $A_{2u}(\Gamma)$. The latter becomes prominent at considerably higher E_i [30] – see Fig 6b for $E_i=3.81 \text{ eV}$. Finally, the fact that the resonant behavior of the α_2 band cannot be exclusively related with $2LA'$ (M) may suggest that $2LA$ (M) band is also enhanced near the excitonic resonance. However, it is noteworthy that at lower temperatures (and $E_i=1.96 \text{ eV}$) the $L_3 / (L_3+L_4)$ intensity ratio is somewhat increased (will be shown elsewhere), which may point to the former being slightly more resonant with respect to the latter.

D. Analysis of infrared-allowed second-order spectrum in bulk $2H\text{-MoS}_2$

The group theoretical analysis done for the Raman scattering is complemented in Tables 1-4 by the analysis of IR activity. Shown in **Fig. 8** an IR absorption spectrum previously measured by Willson and Yoffe for a $180 \mu\text{m}$ layer of $2H\text{-MoS}_2$ (Fig. 39 in [18]). The M point IR-allowed (Raman-forbidden) combinations (Table 3) are also denoted. For the sake of clarity we do not show the K and Γ points IR-active combinations, but we bear in mind that those are also potentially contributors. In black stripes, the absorption bands from Agnihorti [32] are also indicated after subtracting from them 5 cm^{-1} in order to take into account temperature effects (as the reported frequencies [32] are for 77 K). Good correlation between the positions reported in the two studies is evident. We also show proposed assignments to some of the bands. In cases where the M-point phonons of Davydov doublets origins are close in frequencies, there are two allowed combinations with LA/LA' or TA/TA'. For example, $A_{2u}^1(\text{M}) + \text{LA}'(\text{M})$ vs. $B_{2g}^1(\text{M}) + \text{LA}(\text{M})$. In the high side of the spectrum there is a band with similar frequency to that found in the Raman spectrum, but with different symmetry ($2A_{1g}(\text{M})$ - Raman active vs. $A_{1g}(\text{M})+B_{1u}(\text{M})$ –IR active).

E. Symmetry mode analysis of second-order Raman scattering of monolayer *IH*-MoS₂

Similar analysis to that of bulk *2H*-MoS₂ can be made for monolayer *IH*-MoS₂, for which the number of phonon dispersion relations is reduced from 18 to 9. The important differences lie in *i*. The fact that from each of the *2H* Davydov doublets of the optical phonons (B_{2g}^1 & A_{2u}^1), (A_{1g} & B_{1u}), (E_{2g}^1 & E_{1u}^1) and (E_{1g} & E_{2u}) there is one branch left in the Γ point of the *IH* form with A''_2 , A'_1 , E' and E'' symmetries, respectively, *ii*. The branches at the M point, which commence at Γ and originate from the quasi-acoustic phonons of E_{2g}^2 and B_{2g}^2 (LA' , TA' and ZA' phonons), are absent in the monolayer.

In what follows we show the spectral analysis for the monolayer while restricting ourselves to the Γ and M points. The eigenstates at those points correspond to irreducible representations of the point groups D_{3h} and C_{2v} , respectively. **Table 6** lists the various branches with their symmetries at the Γ and M points. In **Table 7** the Raman and IR activity of the various modes are specified and the polarizability tensors of the Raman-active phonons at the Γ point are presented. For the Γ point second-order transitions we find bands, which are either Raman- or IR-active, or both. For the M point all the bands are both Raman- and IR-active. Unlike the phonon energies at Γ , which are mostly known experimentally, at the M point only calculated values are available, which seem to be within a few cm^{-1} from the bulk values [22, 24]. We shall take the corresponding *monolayer* values to be similar to those of the bulk and employ the same procedure described above in tables 1 – 3 (see further details in the supporting information). Although the two are obviously not expected to be truly the same, it may be used as an estimation, in order to provide a guideline for the energies of the second-order transitions of the single layer M and Γ points phonons, which are shown in **Table 8**.

Figure 9a presents the Raman spectrum of monolayer MoS₂, measured at $E_i = 1.96$ eV. Apart from the well-known first-order bands [8-10] we focus on the ‘2LA band’ and compare it to the calculated 2PDOS of the monolayer [22] (after being shifted, for clarity, by a few cm^{-1}). Two distinct bands are apparent, which are also distinguishable in the 2PDOS. Similar to the bulk case, the correlation between the measured Raman and the 2PDOS is quite good. In line with the correlation with 2PDOS we tentatively assign the lower band to a van Hove singularity between K and M, and the higher one to the 2LA (M) and possibly also to a contribution of 2LA(K) (note the absence of LA' phonons).

Recently, Scheuschner *et al.* [33] showed that the room temperature resonance Raman profile of the $A'_1(\Gamma)$ phonon fits nicely to the *A* and *B* excitonic transitions for monolayer MoS₂. In another recent study Pimenta *et al.* [13] presented the Raman scattering excitation energy dependence for

monolayer MoS₂, from where it can be shown that the (α_1/α_2) intensity ratio follows the B excitonic transitions (the lowest excitation energy was 1.95 eV and therefore no conclusion can be drawn for the A exciton, which is centered at ~ 1.84 eV). Hence, unlike the bulk, in the monolayer there is an enhancement of the α_1 intensity with respect to that of α_2 . This result cannot be exclusively related with the absence of the LA' phonons in the monolayer because in the bulk α_2 does not show as well resonant enhancement in the vicinity of the B exciton. Further theoretical clarification is needed to explore the possibility of enhancement in the monolayer of the presumably 2PDOS mode.

In **Fig. 9c** and **9d** we show the spectra of the monolayer in the energy range of and 500-850 cm⁻¹ and 110-280 cm⁻¹, respectively, where second-order transitions are expected. The former is for overtones and combinations and the latter for the corresponding difference spectra. We denote in the figure the 'expected' positions of the various second-order bands that are due to A'₁(M), E'(M₁), E'(M₂) and LA(M) modes. By comparing the monolayer spectra with the bulk off-resonant 1.58 eV spectrum, we find that the two have substantial common characteristics and that the measured peaks correlate well with the expected energies listed in Table 8. It is noteworthy that the 228 cm⁻¹ band, which is absent in the 1.58 eV bulk spectrum, may be attributed to the A'₁(M)-ZA(M) difference band or, as recently proposed [34], to the LA(M) phonon.

F. A suggested reassignment of the 'b band' in MoS₂

In a resonant Raman scattering study on a single crystal of 2H-MoS₂ at $T = 7$ K and in the laser frequency range of $1.9 < E_i < 2.3$ eV, Sekine *et al.* [4] explored a highly dispersive band at 429 cm⁻¹ denoted as the 'b band'. The Stokes peak in that band has been interpreted in terms of a two-phonon process. The first phonon is the E¹_{1u} phonon of finite wavevector and the second a B²_{2g} quasi-acoustic phonon (Δ_2), which involves vibration of the S-Mo-S planes against each other. According to this interpretation the effect of varying the Inorganic Fullerenes (IF) diameter on the shift of the 'b band' was explained by Frey *et al.* [7], and the effect of pressure and temperature on the 'b band' frequency and the ~ 5 cm⁻¹ shift between the Stokes and anti-Stokes frequencies of this band were analyzed in our previous publication [5].

There are two characteristics that should be fulfilled for the 'b band' interpretation [4] to apply: *i.* The exciting laser line is above the level of the A (or B) exciton. *ii.* The existence of the B²_{2g} mode, which appears in the bulk and not in the monolayer. From Fig. 9a it appears that the 'b band' is found in the Raman spectrum of the monolayer. Furthermore, like in the case of the bulk, the center

frequency of the ‘b band’ in the anti-Stokes spectrum also shows a $\sim 5 \text{ cm}^{-1}$ red shift relative to that found in the Stokes spectrum. Moreover, it seems that the intensity of the ‘b band’ in the monolayer shows some excitonic resonant dependence (see Fig. 4 in Ref. 13). As a consequence of these new findings (the actual ‘appearance’ of this band in monolayer and its characteristics), a suggested alternative assignment of the ‘b band’ is desirable. With the aid of the newly constructed Table 3 we seek for a possible attribution of the transitions that are found at low temperatures in bulk MoS₂ at $\sim 423 \text{ cm}^{-1}$ and $\sim 428 \text{ cm}^{-1}$ in anti-Stokes and Stokes spectra, respectively [4, 5].

For the M point the only possible attribution is LA (M) + ZA (M) at $\sim 417 \text{ cm}^{-1}$, which is too low with respect to the experimental values. For the K point we find LA’ (K)+TA (K) /TA ‘(K) at $\sim 427 \text{ cm}^{-1}$, and LA (K)+TA (K) /TA ‘(K) at $\sim 424 \text{ cm}^{-1}$, which are within the expected frequencies and are also shifted by $\sim 3 \text{ cm}^{-1}$. We also note that LA’ (K)+ZA (K)/ZA ‘(K) and LA (K)+ZA (K)/ZA ‘(K) (which contain only the E_{1g}(Γ) representation in our scheme) are expected at $\sim 422 \text{ cm}^{-1}$, and $\sim 419 \text{ cm}^{-1}$, respectively. Although the frequencies at the K point had not been satisfactorily verified to match the experimental data (since most of the attributed transitions are from the M point), we can still suggest that the ‘b band’ is more likely related with second-order phonon at the K point.

We may therefore suggest that the ‘b band’ is constructed from two bands, for which their peaks were not well separable in previous studies [4, 5, 7]: the higher band/s (LA’ (K)+ TA (K)/TA ‘(K) or LA (K)+TA (K)/TA ‘(K)) is resonant with the *A* exciton and is more pronounced in the Stokes outgoing resonance [5], and the lower band is constructed from the contribution/s of combination band/s: LA’(K)+ ZA(K)/ZA’(K) or LA (K)+ZA (K)/ZA ‘(K). For the monolayer case the phonons LA(K)+TA(K) and LA(K)+ ZA(K) may be considered. Hence, the resonant activation of the upper band (that is minor in the anti-Stokes side) may be related with what we considered as a large blue shift of this mode in the Stokes with respect to the ‘less resonant’ anti-Stokes side.

Additional support of the proposed reassignment can be found in **Figure 9b**, which compares the Stokes and anti-Stokes spectra of 2H-MoS₂, measured at E_i = 1.58 eV and at room temperature. There are clearly two weak bands at ~ 422 and $\sim 417 \text{ cm}^{-1}$, in the similar spectral positions of the room temperature ‘b band’ in the Stokes and anti-Stokes spectra, measured at E_i = 1.96 eV. The appearance of these bands, which are presumably correlated with the ‘b band’, is not consistent with the full requirements needed for the currently available interpretation [4, 5, 7] to be valid. This is because E_i is significantly lower than the *A* exciton energy. Furthermore, it seems that unlike for the resonant E_i=1.96 eV case, the $\sim 5 \text{ cm}^{-1}$ shift between the two major bands is not observed in the spectra of E_i = 1.58 eV and the two modes appear in about the same spectral positions in both Stokes and anti-Stokes spectra. This new proposed alternative interpretation of the ‘b band’ remains to be

substantiated further. It is particularly important (and challenging) to separate the seemingly hardly-resolved contributions of the sub-bands that construct the ‘b band’ in spectra measured under resonance.

4. Conclusions

To summarize, we present a comprehensive analysis of multiphonon Raman spectrum in MoS₂. The low temperature resonant spectra were measured with excitation energy of 1.96 eV, which is slightly shifted in energy from the *A* exciton. The analysis consists of symmetry assignments, from which we obtain a broad set of allowed second-order transitions at high-symmetry points in the Brillouin zone.

1. An important physical insight from this study, is that in the bulk the majority of multiphonon resonant bands are proposed to originate from combination processes between four BZ edge phonons at M that are from branches that are optical at Γ (with $A_{1g}(\Gamma)$, $E^1_{2g}(\Gamma)$ and $E^2_{2g}(\Gamma)$). Consistent with the fact that at the M Brillouin edge only combinations with the same inversion symmetry (*g* or *u*) are Raman-allowed, the contribution of combinations with the LA (M) mode can not be considered with the four phonons that were assigned to construct the ‘resonant group’ $A_{1g}(M)$, $E^1_{2g}(M_2)$, $E^2_{2g}(M_1)$ (TA’ (M)) and $E^2_{2g}(M_2)$ (LA’ (M)). Among those four phonons, all (but one, which is not experimentally detectable in our system) of the 2nd order overtones, combination and difference-bands and many of the third order bands are found in the low temperature resonant Raman spectra.

2. As a complemented study we extended the analysis infrared allowed second-order transitions. We also present a multiphonon analysis of the M and Γ points for monolayer *IH*-MoS₂. Correlation between the analysis and room temperature Raman spectrum measured at 1.96 eV is satisfactory.

3. We demonstrate that the ‘2LA band’ at $\sim 460 \text{ cm}^{-1}$ measured at 1.16-2.41 eV is constructed from at least five Lorentzian contributions. Supported by the striking similarity between this band, measured under off-resonant conditions, and the 2PDOS [22], we propose the reassignment of the lower part of the band (α_1), that was previously attributed to 2LA(M), to a van Hove singularity between K and M and the higher part (α_2) to mostly the overtones of the LA and LA’ phonons at the M point. The $A_{2u}(\Gamma)$ mode is activated under excitations with considerably higher energy of 3.81 eV (and evidently also with 2.81 eV [30]). Similar approach applies for monolayer *IH*-MoS₂.

We anticipate that this analysis will promote the understanding of the currently unresolved mechanism of the multiphonon scattering in MoS₂ and its intricate excitation energy dependence. It may as well inform the interpretation of similar processes from a range of other layered dichalcogenides.

5. Acknowledgments

We thank Dr. Leila Zeiri from Ben-Gurion University for assistance with acquiring the low temperature and the UV Raman spectra. We also acknowledge the use of the Raman spectrometer under room temperature conditions in the Centralized Research Facilities at Drexel University and Dr. Zhorro Nikolov for his assistance. We gratefully acknowledge Dr. Feng Yan for helping with topographic scanning probe microscopy of the monolayer sample and Vladimir Bačić for sharing his preliminary dispersion curves calculations. Work at Drexel was supported by the National Science Foundation and the Semiconductor Research Corporation (DMR 1124696).

* Corresponding author e-mail: T.Livneh@nrcn.org.il

#Part of the work was done during a Sabbatical leave at the Department of Materials Science & Engineering, Drexel University, USA.

6. References

1. T.J. Wieting and J.L. Verble, *Phys. Rev. B* 3, 4286 (1971)
2. J. M. Chen and C. S. Wang, *Solid State Commun.*, 14, 857 (1974)
3. A. M. Stacy and D. T. Hodul, *J. Phys. Chem. Solids* 46, 405 (1985)
4. T. Sekine, K. Uchinokura, T. Nakashizu, E. Matsuura, and R. Yoshizaki, *J. Phys. Soc. Jpn.* 53, 811 (1984). ; T. Sekine, T. Nakashizu, M. Izumi, K. Toyoda, K. Uchinokura, E. Matsuura, *J. Phys. Soc. Jpn.* 49 Suppl. A, 551 (1980).
5. T. Livneh and E. Sterer, *Phys. Rev. B* 81, 195209 (2010).
6. J.-H. Fan, P. Gao, A.-M. Zhang, B.-R. Zhu, H.-L. Zeng, X.-D. Cui, R. He, and Q.-M. Zhang, *J. Appl. Phys.*, 115, 053527 (2014)
7. G. L. Frey, R. Tenne, M.J. Matthews, M. S. Dresselhaus, and G. Dresselhaus, *Phys. Rev. B* 60, 2883 (1999)
8. C. Lee, H. Yan, L. E. Brus, T. F. Heinz, J. Hone, S. Ryu, *ACS Nano*, 4, 2695 (2010)
9. B. Chakraborty, H. S. S. R. Matte, A. K. Sood, and C. N. R. Rao, *J. Raman Spectrosc.*, 44, 92 (2013)
10. H. Li, Q. Zhang, and C. Yap, *Adv. Funct. Mat.* 22, 1385 (2012)
11. Y. Zhao, X. Lou, H. Li, J. Zhang, P. T. Araujo, C.K. Gan, J. Wu, H. Zhang, S.Y. Quek, M.S. Dresselhaus, Q. Xiong *Nanoletters* 13 1007 (2013)
12. X. Zhang, W. P. Han, J. B. Wu, S. Milana, Y. Lu, Q. Q. Li, A. C. Ferrari, P.H. Tan *Phys. Rev. B* 87, 115413 (2013).

13. M. A. Pimenta, E. del Corro, B. R. Carvalho, C. Fantini, and L. M. Malard, *Acc. Chem. Res.* 48(1), 41 , (2015).
14. K. Gołasa, M. Grzeszczyk, P. Leszczyński, C. Faugeras, a. a. L. Nicolet, a. Wysmołek, M. Potemski, and a. Babiński, *Appl. Phys. Lett.*, 104, 092106, (2014).
15. K. Gołasa, M. Grzeszczyk , K. P. Korona, R. Bożek, J. Binder, J. Szczytko, A. Wysmołek, *Acta Phys. Pol. A* 124, 849, (2013).
16. K. F. Mak , C. Lee , J. Hone , J. Shan , T. F. Heinz , *Phys. Rev. Lett.*, 105, 136805 (2010).
17. C. Sourisseau, F. Cruge, and M. Fouassier, *Chem. Phys.* 150, 281 (1991).
18. J.A. Wilson and A.D. Yoffe , *Adv. Phys.* 18 193 (1969)
19. N.W. Wakabayashi, H.G. Smith and R.M. Nicklow *Phys. Rev. B* 12, 659 (1975)
20. D.L. Rousseau, R.P. Bauman, S.P.S. Porto *J. Raman Spectrosc.*, 10, 253 (1981)
21. R. S. Mulliken, *J. Chem. Phys.* , 23, 1997 (1955); 24, 1118 (1956).
22. C. Ataca, M. Topsakal, E. Akt, and S. Ciraci, *J. Phys. Chem. C* 115, 16354 (2011).
23. A. P. S. Gaur, S.Sahoo, M. Ahmadi, M. J.-F. Guinel, S. K. Gupta, R. Pandey, S. K. Dey, R. S. Katiyar *J. Phys. Chem. C* 117, 26262 (2013)
24. A. Molina-Sánchez and L. Wirtz *Phys. Rev. B* 84, 155413 (2011)
25. a. E.B. Wilson, J.C. Decius and P.C. Cross “*Molecular vibrations*” (Dover, N.Y. 1980) p. 331. b. M. Cardona, in *Light Scattering in Solids II*, edited by M. Cardona and G. Güntherodt (Springer-Verlag, Berlin, 1983), p. 19.
26. Aroyo M.I., A. Kirov, C. Capillas, J. M. Perez-Mato & H. Wondratschek, *Acta Cryst.* A62 115 (2006); <http://www.cryst.ehu.es>.
27. M.S. Dresselhaus, G. Dresselhaus, A. Jorio, ”*Group theory, Application to the Physics of Condensed Matter*” (Springer, Berlin 2008) p. 209
28. H. Zeng, B. Zhu, K. Liu, J. Fan, X. Cui, Q.M. Zhang *Phys. Rev. B* 86, 241301(R) (2012)
29. D. Y. Qiu, F. H. da Jornada, and S. G. Louie, *Phys. Rev. Lett.* 111, 216805 (2013)
30. J. Lee, J. Park, Y. Son and H. Cheong, *Nanoscale*, 7, 3229 (2015)
31. An attempt to fit this band with less than five sub-bands was not successful. One cannot exclude the possibility of more than five contributions. Within our proposed scheme for the spectrum with $E_i=1.58$ eV the widths of the L_1 - L_5 bands are 17.4, 9.1, 8.3, 8.6 and 6.3 cm^{-1} , respectively. For comparison, the widths of the $E_{12g}^1(\Gamma)$ and $A_{1g}(\Gamma)$ bands are: 2.7 and 2.8 cm^{-1} . The width of the $A_{2u}(\Gamma)$ band, measured with $E_i=3.81$ eV, is ~ 3.9 cm^{-1} .
32. O.P. Agnihorti *J. Phys. Chem. Solids* 33 1173 (1972)
33. N. Scheuschner, O. Ochedowski, M. Schleberger, and J. Maultzsch *phys. stat. sol.(b)* 249, 2644 (2012)
34. S. Mignuzzi, J.A. Pollard, N. Bonini, B. Brennan, I.S. Gilmore, M.A. Pimenta, D. Richards, and D. Roy *Phys. Rev. B* . 91, 195411 (2015)

Tables and Figures

Table 1 A list of phonons of 2H-MoS₂, their symmetry assignments and frequencies for high-symmetry point of Γ , M (left) and K (right) in the Brillouin zone.

Band	Γ/D_{6h}	$\nu(\text{cm}^{-1})^*$	Band		M/D_{2h}	$\nu(\text{cm}^{-1})^\#$	Band		K/D_{3h}	$\nu(\text{cm}^{-1})^\#$
<i>A (N)</i>	B_{2g}^1	475	α	$B_{2g}^1 M$	B_{3g}	393	a	$B_{2g}^1 K$	A_2'	380
<i>B (IR)</i>	A_{2u}^1	470	β	$A_{2u}^1 M$	B_{1u}	393	b	$A_{2u}^1 K$	A_2'	380
<i>C (R)</i>	A_{1g}	409	χ	$A_{1g} M$	A_g	412	c	$A_{1g} K$	A_1'	402
<i>D (N)</i>	B_{1u}	403	δ	$B_{1u} M$	B_{2u}	411	d	$B_{1u} K$	A_1'	402
<i>E (IR)</i>	E_{1u}^1	384	ε_1	$E_{1u}^1 M_1$	B_{2u}	370	e	$E_{1u}^1 K_1$	A_1'	388
			ε_2	$E_{1u}^1 M_2$	B_{3u}	362	g	$E_{ug} K_2$	E'	341
<i>F (R)</i>	E_{2g}^1	383	ϕ_1	$E_{2g}^1 M_1$	B_{2u}	362	f	$E_{2g}^1 K_2$	A_1'	385
			ϕ_2	$E_{2g}^1 M_2$	A_g	370				
<i>G (N)</i>	E_{2u}	297	γ_1	$E_{2u} M_1$	B_{1u}	338	h	$E_{2u} K_1$	A_2'	338
			γ_2	$E_{2u} M_2$	A_u	303	j	$E_{ug} K_1$	E''	330
<i>H (R)</i>	E_{1g}	286	η_1	$E_{1g} M_1$	B_{2g}	306	i	$E_{1g} K_2$	A_2'	342
			η_2	$E_{1g} M_2$	B_{3g}	330				
<i>I (N)</i>	B_{2g}^2	58	ι	$B_{2g}^2 M$ (ZA')	B_{3g}	174	k	$B_{2g}^2 K$ (ZA')	A_2'	184
<i>J (R)</i>	E_{2g}^2	35	φ_1	$E_{2g}^2 M_1$ (TA')	B_{1g}	160	l	$E_{2g}^2 K_1$ (TA')	A_2''	188
			φ_2	$E_{2g}^2 M_2$ (LA')	A_g	233	m	$E_{2g}^2 K_2$ (LA')	A_1'	237
<i>K (AC)</i>	E_{1u}^2		κ_1	$E_{1u}^2 M_1$ (LA)	B_{2u}	235	n	$E_{1u}^2 K_2$ (LA)	A_1'	234
			κ_2	$E_{1u}^2 M_2$ (TA)	B_{3u}	156	o	$E_{1u}^2 K_1$ (TA)	A_2''	190
<i>L (AC)</i>	A_{2u}^2		λ	$A_{2u}^2 M$ (ZA)	B_{1u}	182	p	$A_{2u}^2 K$ (ZA)	A_2'	185

* Measured values at ~ 300 K [1-3]

Proposed values at low temperatures (see text)

Table 2 Group theoretical selection rules for two-phonon Raman and IR activity from the Γ , M and K Brillouin zone points in bulk $2H$ -MoS₂. The two active groups of symmetries are denoted with different colors. The scattering tensors of the Raman-active phonons are also shown ($c=d$ away from resonance [25b]).

Γ						M					K						
Phonon combination	A_{1g}	E_{1g}	E_{2g}	A_{2u}	E_{1u}	Phonon combination	A_{1g}	E_{1g}	E_{2g}	A_{2u}	E_{1u}	Phonon combination	A_{1g}	E_{1g}	E_{2g}	A_{2u}	E_{1u}
	$A_{1g} \times A_{1g}$	X						$A_g \times A_g$	X		X				$A_1 \times A_1$	X	
$A_{1g} \times A_{2u}$				X		$A_g \times A_u$				X		$A_1 \times A_1$		X			
$A_{1g} \times B_{2g}$						$A_g \times B_{1g}$	X		X			$A_1 \times A_2$		X		X	
$A_{1g} \times B_{1u}$						$A_g \times B_{1u}$				X		$A_1 \times A_2$			X	X	X
$A_{1g} \times E_{1g}$		X				$A_g \times B_{2g}$		X				$A_1 \times E$			X		X
$A_{1g} \times E_{2g}$			X			$A_g \times B_{2u}$				X		$A_1 \times E$		X			
$A_{1g} \times E_{1u}$					X	$A_g \times B_{3g}$		X				$A_1 \times A_1$	X		X		X
$A_{1g} \times E_{2u}$						$A_g \times B_{3u}$				X		$A_1 \times A_2$			X	X	X
$A_{2u} \times A_{2u}$	X					$A_u \times A_u$	X		X			$A_1 \times A_2$		X			
$A_{2u} \times B_{2g}$						$A_u \times B_{1g}$				X		$A_1 \times E$			X		X
$A_{2u} \times B_{1u}$						$A_u \times B_{1u}$	X		X			$A_1 \times E$		X			
$A_{2u} \times E_{1g}$					X	$A_u \times B_{2g}$					X	$A_2 \times A_2$	X		X		X
$A_{2u} \times E_{2g}$						$A_u \times B_{2u}$		X				$A_2 \times A_2$		X			
$A_{2u} \times E_{1u}$		X				$A_u \times B_{3g}$					X	$A_2 \times E$		X			
$A_{2u} \times E_{2u}$			X			$A_u \times B_{3u}$		X				$A_2 \times E$			X		X
$B_{2g} \times B_{2g}$	X					$B_{1g} \times B_{1g}$	X		X			$A_2 \times A_2$	X		X		X
$B_{2g} \times B_{1u}$				X		$B_{1g} \times B_{1u}$				X		$A_2 \times E$		X			
$B_{2g} \times E_{1g}$			X			$B_{1g} \times B_{2g}$		X				$A_2 \times E$			X		X
$B_{2g} \times E_{2g}$		X				$B_{1g} \times B_{2u}$				X		$E \times E$	X	X	X		X
$B_{2g} \times E_{1u}$						$B_{1g} \times B_{3g}$		X				$E \times E$			X	X	X
$B_{2g} \times E_{2u}$					X	$B_{1g} \times B_{3u}$				X		$E \times E$	X	X	X		X
$B_{1u} \times B_{1u}$	X					$B_{1u} \times B_{1u}$	X		X								

$B_{1u} \times E_{1g}$					$B_{1u} \times B_{2g}$				X	Raman active
$B_{1u} \times E_{2g}$				X	$B_{1u} \times B_{2u}$		X			IR active
$B_{1u} \times E_{1u}$			X		$B_{1u} \times B_{3g}$				X	$A_{1g} = \begin{bmatrix} a & 0 & 0 \\ 0 & a & 0 \\ 0 & 0 & b \end{bmatrix}$ $E_{1g} = \begin{bmatrix} 0 & 0 & -c \\ 0 & 0 & c \\ -d & d & 0 \end{bmatrix}$ $E_{2g} = \begin{bmatrix} e & e & 0 \\ e & -e & 0 \\ 0 & 0 & 0 \end{bmatrix}$
$B_{1u} \times E_{2u}$		X			$B_{1u} \times B_{3u}$		X			
$E_{1g} \times E_{1g}$	X		X		$B_{2g} \times B_{2g}$	X		X		
$E_{1g} \times E_{2g}$		X			$B_{2g} \times B_{2u}$				X	
$E_{1g} \times E_{1u}$				X	$B_{2g} \times B_{3g}$	X		X		
$E_{1g} \times E_{2u}$					$B_{2g} \times B_{3u}$				X	
$E_{2g} \times E_{2g}$	X		X		$B_{2u} \times B_{2u}$	X		X		
$E_{2g} \times E_{1u}$					$B_{2u} \times B_{3g}$				X	
$E_{2g} \times E_{2u}$				X	$B_{2u} \times B_{3u}$	X		X		
$E_{1u} \times E_{1u}$	X		X		$B_{3g} \times B_{3g}$	X		X		
$E_{1u} \times E_{2u}$		X			$B_{3g} \times B_{3u}$				X	

Table 3 A proposed complete set of second-order phononic transitions from M and K BZ points in $2H\text{-MoS}_2$. Different groups of Raman scattering tensors are denoted, in accordance with Tables 1 and 2, and are marked with different background colors. The upper number is for a combination and the lower one for a difference band (which are not shown below 70 cm^{-1}). In thick blue frames we denote M point Raman allowed resonant second-order processes. The M point IR-allowed combinations are denoted with white background.

393	174 ZA'	393	412	411	370	362	362	370	160 TA'	233 LA'	338	303	306	330	235 LA	156 TA	182 ZA		
$B_{\text{M}}^{1_{2g}}$	$B_{\text{M}}^{2_{2g}}$	$A_{\text{M}}^{1_{2u}}$	$A_{\text{M}}^{1_{1g}}$	$B_{\text{M}}^{1_{1u}}$	$E_{\text{M}_1}^{1_{1u}}$	$E_{\text{M}_2}^{1_{1u}}$	$E_{\text{M}_1}^{1_{2g}}$	$E_{\text{M}_2}^{1_{2g}}$	$E_{\text{M}_1}^{2_{2g}}$	$E_{\text{M}_2}^{2_{2g}}$	$E_{\text{M}_1}^{2_{2u}}$	$E_{\text{M}_2}^{2_{2u}}$	$E_{\text{M}_1}^{1_{1g}}$	$E_{\text{M}_2}^{1_{1g}}$	$E_{\text{M}_1}^{2_{1u}}$	$E_{\text{M}_2}^{2_{1u}}$	$A_{\text{M}}^{2_{2u}}$	M D2h	
786	567 219	786	805	804	763	755	755	763	553 233	626 160	731	696 90	699 87	723	628	549	575	$B_{\text{M}}^{1_{2g}}$	B_{3g}
	348	567	586 238	585	544	536	536	544 196	334	407	512	477 129	480 132	504 156	409	330	356	$B_{\text{M}}^{2_{2g}}$	B_{3g}
		786	805	804	763	755	755	763	553	626	731	696	699	723	628 158	549 237	575 211	$A_{\text{M}}^{1_{2u}}$	B_{1u}
			824	823	782	774	774	782	572 252	645 179	750	715 109	718 106	742 82	647	568	594	A_{1g}	A_g
$A_{\text{K}}^{2_{2u}}$	370			822	781	773	773	781	571	644	749 73	714	717	741	646 176	567 255	593 229	B_{1u}	B_{2u}
$B_{\text{K}}^{2_{2g}}$	370	370			740	732	732	740	530	603	708	673	676	700	605 135	526 212	552 188	$E_{\text{M}_1}^{1_{1u}}$	B_{2u}
$E_{\text{K}_1}^{2_{1u}}$	375	375	380			724	724	732	522	609	700	665	668	692	597 127	518 206	544 180	$E_{\text{M}_2}^{1_{1u}}$	B_{3u}
$E_{\text{K}_2}^{2_{2g}}$	375	375	380	380			724	732	522	595	700	665	668	692	597 127	518 206	544 180	$E_{\text{M}_1}^{1_{2g}}$	B_{2u}
$E_{\text{K}_2}^{2_{1u}}$	419	419	424	424	468			740	530 210	603 137	708	673	676	700	605	526	552	$E_{\text{M}_2}^{1_{2g}}$	A_g
$E_{\text{K}_2}^{2_{2g}}$	422	422	427	427	471	474			320	393 73	498	463 143	466 146	490 170	395	316	342	$E_{\text{M}_1}^{2_{2g}}$	B_{1g}
$E_{\text{K}_1}^{u_{2g}}$	515 145	515 145	520 140	520 140	564 96	567 93	660			466	571	536 70	539 73	563 97	468	389	415	$E_{\text{M}_2}^{2_{2g}}$	A_g
$E_{\text{K}_1}^{2_{2u}}$	523 153	523 153	528 148	528 148	572 104	575 101	668	676			676	641	644	668	573 103	494 182	520 156	E_{2u}	B_{1u}
$E_{\text{K}_2}^{u_{2g}}$	526 156	526 156	531 151	531 151	575 107	578 104	671	679	682			606	609	633	538	459	485	E_{2u}	B_{3g}
$E_{\text{K}_2}^{1_{1g}}$	527 157	527 157	532 152	532 152	576 108	579 105	672	680	683	684			612	636	541	462	488	E_{1g}	B_{2g}
$A_{\text{K}}^{1_{2u}}$	565 195	565 195	570 190	570 190	614	617	710	718	721	722	760			660	565	486	512	E_{1g}	B_{3g}
$B_{\text{K}}^{1_{2g}}$	565 195	565 195	570 190	570 190	614 146	617 143	710	718	721	722	760	760			470	389 79	417	$E_{\text{M}_1}^{2_{1u}}$	B_{2u}
$E_{\text{K}_2}^{1_{2g}}$	570 200	570 200	575 195	575 195	619 151	622 148	715	723	726	727	765	765	770			312	338	$E_{\text{M}_2}^{1_{1u}}$	B_{3u}
$E_{\text{K}_1}^{1_{1u}}$	573 203	573 203	578 198	578 198	622 154	625 151	718	726	729	730	768	768	773	776			364	$A_{\text{M}}^{2_{2u}}$	B_{1u}
$B_{\text{K}}^{1_{1u}}$	587 217	587 217	592 212	592 212	633 168	636 165	732 72	740	743	744	782	782	787	791	804			E_{1g}	
$A_{\text{K}}^{1_{1g}}$	587 217	587 217	592 212	592 212	633 168	639 165	732 72	740	743	744	782	782	787	791	804	804		E_{2g}	
K D3h	$A_{\text{K}}^{2_{2u}}$	$B_{\text{K}}^{2_{2g}}$	$E_{\text{K}_1}^{2_{1u}}$	$E_{\text{K}_2}^{2_{2g}}$	$E_{\text{K}_2}^{2_{1u}}$	$E_{\text{K}_2}^{2_{2g}}$	$E_{\text{K}_1}^{u_{2g}}$	E_{2u}	$E_{u_{2g}}$	E_{1g}	$A_{\text{K}}^{1_{2u}}$	$B_{\text{K}}^{1_{2g}}$	$E_{\text{K}_2}^{1_{2g}}$	$E_{\text{K}_1}^{1_{1u}}$	B_{1u}	A_{1g}		A_{1g}, E_{2g}	
	185 ZA	185 ZA'	190 TA	190 TA'	234 LA	237 LA'	330	338	341	342	380	380	385	388	402	402		E_{1g}, E_{2g}	
	A_2'	A_2'	A_2''	A_2''	A_1'	A_1'	E''	A_2'	E'	A_2'	A_2'	A_2'	A_1'	A_1'	A_1'	A_1'		A_{1g}, E_{1g}, E_{2g}	

Table 4 Raman (colored) and IR (white) active combinations for second-order processes from phonons at Γ in $2H$ -MoS₂ measured at 300 K. Different groups of Raman scattering tensors are denoted, in accordance with Tables 1 and 2 and marked with different background colors. The upper number is for a combination and the lower one for a difference band (which are not shown below 70 cm⁻¹). The x sign denotes an inactive combination.

A _{1g} 409	A _{2u} 470	B ¹ _{2g} 475	B ² _{2g} 58	B _{1u} 403	E ¹ _{2g} 383	E ² _{2g} 35	E _{1g} 286	E _{1u} 384	E _{2u} 297	Γ/D_{6h}
818	879	x	x	x	792	444 374	695 123	793	x	A _{1g} 409
	940	x	x	x	x	x	756	854 86	767 173	A _{2u} 470
		950	533 417	878	858 92	510 440	761 189	x	772	B ¹ _{2g} 475
			116	461	441 325	93	344 228	x	355	B ² _{2g} 58
				806	786	438	x	787	800 106	B _{1u} 403
					766	418 348	669 97	767	680	E ¹ _{2g} 383
		A _{1g}				70	321 251	419	332	E ² _{2g} 35
		A _{1g} , E _{2g}					572	670	583	E _{1g} 286
		E _{1g}						768	681 87	E _{1u} 384
		E _{2g}							594	E _{2u} 297

Table 5 Proposed assignments of 2H-MoS₂ at low temperature (95 K), measured up to 1130 cm⁻¹ using excitation energy of 1.96 eV. The notations are shown in Table 1*.

$\nu(\text{cm}^{-1})$	Assignment	$\nu(\text{cm}^{-1})$	Assignment	$\nu(\text{cm}^{-1})$	Assignment
88	$\varphi_1^2\bar{\varphi}_2$	405.5	<i>D</i>	739	ϕ_2^2
92	$\bar{\varphi}_1^2\chi$	411	<i>C</i>	756	$\beta\epsilon_2$
96	$\varphi_2^2\bar{\phi}_2$	428	#	768	f^2
115	I^2	456	$\$$	781.5	$\phi_2\chi$
118	$\varphi_1\phi_2\bar{\chi}$	466	φ_2^2	788	$\varphi_1^2\varphi_2^2, \alpha^2, \beta^2$
125	$\gamma_2\bar{\nu}, \epsilon_2\bar{\kappa}_1$	470	κ_1^2	794.5	de, ce
137	$\bar{\varphi}_2\phi_2$	478	k^2	802	$\chi\alpha$
142	$\varphi_1^2\varphi_2\bar{\chi}$	479	φ_1^3	808	$\varphi_1\varphi_2\chi$
151	$h\bar{l}$	485	$\bar{\varphi}_1\varphi_2\chi$	824	χ^2, C^2, δ^2
159	$\gamma_1\bar{\lambda}$	501.5	$\bar{\varphi}_1^2\chi^2$	836	$\varphi_2^2\phi_2$
168	$c\bar{m}$	514.5	-	850	$\varphi_1^3\phi_2$
180.5	$\varphi_2\bar{\chi}$	530	$\varphi_1\phi_2$	864	$\bar{\phi}_2\chi^3$
192.5	$\phi_2\bar{l}$	546	$\phi_2\iota$	877	$\varphi_2^2\chi$
202	$\varphi_1\bar{\phi}_2\chi$	560.5	$\varphi_2\phi_2^2\bar{\chi}$	892	$\varphi_1^3\chi$
210	$\bar{\varphi}_1\phi_2$	566	$\iota\alpha$	901-947	$\varphi_2^4, \varphi_1\phi_2\chi \dots$
229	$\delta\bar{\lambda}, H\bar{l}$	573	$\varphi_1\chi$	958	$\bar{\varphi}_2\phi_2\chi^2$
236.5	$\bar{\nu}\chi$	576	$\beta\lambda, H^2$	973	$\varphi_2\phi_2^2$
245	$\delta\bar{\kappa}_2$	581	$\bar{\varphi}_1\phi_2^2$	984	$\varphi_1\chi^2$
254	$\bar{\varphi}_1\chi$	591	$\bar{\varphi}_2\chi^2$	1000	$\bar{\varphi}_2\chi^3$
312	κ_2^2	603	$\varphi_2\phi_2$	1013	$\varphi_2\phi_2\chi$
319.5	φ_1^2	620	$\bar{\varphi}_1\varphi_2\chi$	1026	$\varphi_2^3\phi_2^2\bar{\chi}$
329	$\phi_2^2\bar{\chi}$	626	$\varphi_1\varphi_2^2, \varphi_2\alpha$	1030	$\bar{\varphi}_1\phi_2\chi^2$
340	$\varphi_1\bar{\varphi}_2\chi, \kappa_2\lambda$	632	$cm, \eta_1\eta_2$	1043	$\bar{\varphi}_1\varphi_2^2\phi_2^2$
347	ι^2	646	$\varphi_2\chi$	1055	$\varphi_2\chi^2$
356	$\bar{\varphi}_2^2\chi^2$	662	$\bar{\varphi}_1\chi^2$	1061	$\varphi_1^2\phi_2^2$
365	λ^2	677	γ_1^2	1071	$\varphi_2^3\phi_2$
383	$l^2, o^2 ?$	684	i^2	1111	$\varphi_2^3\chi, \phi_2^3$
386.5	<i>F</i>	691	$\varphi_1^2\phi_2$	1117	-
392.5	$\kappa_1\kappa_2$	700	φ_2^3	1130	$\varphi_1\varphi_2\phi_2^2$
394.5	$\varphi_1\varphi_2$	709	-		
398.5	-	725.5	ϕ_1^2		

* x and \bar{x} stand for addition and subtraction of a first-order x phonon and n in x^n represents the order of the multiphonon transition of the x phonon.

The ‘b band’ [4, 5, 7] – see below in Section 3F.

$\$$ See below the attribution of the ‘2LA band’ in Section 3C.

Table 6 A list of phonons of *IH*-MoS₂, their symmetry assignments and frequencies for Γ and M points in the Brillouin zone.

Band	Γ/D_{3h}	$\nu(\text{cm}^{-1})$	Band	$\# \nu(\text{cm}^{-1})$	M/C_{2v}
<i>A</i> (<i>IR</i>)	A_2''	$\sim 470^{**}$	$A_2'' M$	393	B_1
<i>B</i> (<i>R</i>)	A_1'	403*	$A_1' M$	412	A_1
<i>C</i> (<i>IR+R</i>)	E'	384*	$E' M_1$	370	A_1
			$E' M_2$	362	B_2
<i>D</i> (<i>R</i>)	E''	$\sim 273^{**}$	$E'' M_1$	306	A_2
			$E'' M_2$	330	B_1
<i>E</i> (<i>AC</i>)	E'	0	$E' M_1$	235	A_1
			(<i>LA</i>) $E' M_2$	160	B_2
			(<i>TA</i>) $E' M_2$		
<i>F</i> (<i>AC</i>)	A_2''	0	$A_2'' M$	182	B_1
			(<i>ZA</i>) $A_2'' M$		

Measured (*) [8-10] or estimated (**) values at ~ 300 K.

#The frequencies for the M point are estimated.

Table 7 Group theoretical selection rules for two-phonon Raman and IR activity from the Γ and M Brillouin zone points of monolayer $1H$ -MoS₂. The three active groups of symmetries are denoted with different colors. The scattering tensors of the Raman-active phonons are also shown ($c=d$ away from resonance [25b]).

Γ					M				
Phonon combination	A_1	E''	E'	A_2	Phonon combination	A_1	E''	E'	A_2
	$A_1 \times A_1$	X					$A_1 \times A_1$	X	X
$A_1 \times A_1$					$A_1 \times A_2$		X	X	X
$A_1 \times A_2$					$A_1 \times B_1$	X	X	X	
$A_1 \times A_2$				X	$A_1 \times B_2$		X	X	X
$A_1 \times E$			X		$A_2 \times A_2$	X	X	X	
$A_1 \times E''$		X			$A_2 \times B_1$		X	X	X
$A_1 \times A_1$	X				$A_2 \times B_2$	X	X	X	
$A_1 \times A_2$				X	$B_1 \times B_1$	X	X	X	
$A_1 \times A_2$					$B_1 \times B_2$		X	X	X
$A_1 \times E$		X			$B_2 \times B_2$	X	X	X	
$A_1 \times E''$			X						
$A_2 \times A_2$	X					Raman active			
$A_2 \times A_2$						Raman & IR active			
$A_2 \times E$			X			IR active			
$A_2 \times E''$		X				$A_1' = \begin{bmatrix} a & 0 & 0 \\ 0 & a & 0 \\ 0 & 0 & b \end{bmatrix}$ $E'' = \begin{bmatrix} 0 & 0 & -c \\ 0 & 0 & c \\ -d & d & 0 \end{bmatrix}$ $E' = \begin{bmatrix} e & e & 0 \\ e & -e & 0 \\ 0 & 0 & 0 \end{bmatrix}$			
$A_2 \times A_2$	X								
$A_2 \times E$		X							
$A_2 \times E''$			X						
$E \times E$	X		X						
$E \times E''$		X		X					
$E \times E''$	X		X						

Table 8 A complete set of second-order phononic transitions from M and Γ Brillouin zone points in monolayer $1H$ -MoS₂. The upper number is for a combination and the lower one for a difference band (which are not shown below 70 cm⁻¹). The frequencies of the M point are the estimated ones (based on the assumed close resemblance of the $1H$ and $2H$ frequencies). Different groups of Raman scattering tensors are denoted, in accordance with Tables 6 and 7 and are marked with different background colors.

		393	412	370	362	306	330	235	160	182	
	A''_2	A'_1	E'	E'	E''	E''	E'	E'	A''_2	A''_2	M
	M	M	M_1	M_2	M_1	M_2	M_1	M_2	M	M	C_{2v}
		786	805	763	755	699 87	723	628 158	553 233	575 211	A''_2 M
			824	782	774	718 106	742 82	647 177	572 252	594 230	A'_1 M
				740	732	676	700	605 135	530 210	552 188	E' M_1
			E'', E'		724	668	706	597 127	522 202	544 180	E' M_2
			A'_1, E'', E'			612	636	541 71	466 146	488 124	E'' M_1
470	A''_2	940	A'_1, E'				660	565 95	490 170	512 148	E'' M_2
403	A'_1	873	806	E'				470	395 75	417	E' M_1
384	E'	854 86	787	768	E''				320	342	E' M_2
280	E''	750 190	783 127	664 104	560	A'_1				364	A''_2 M
	Γ D_{3h}	A''_2	A'_1	E'	E''						

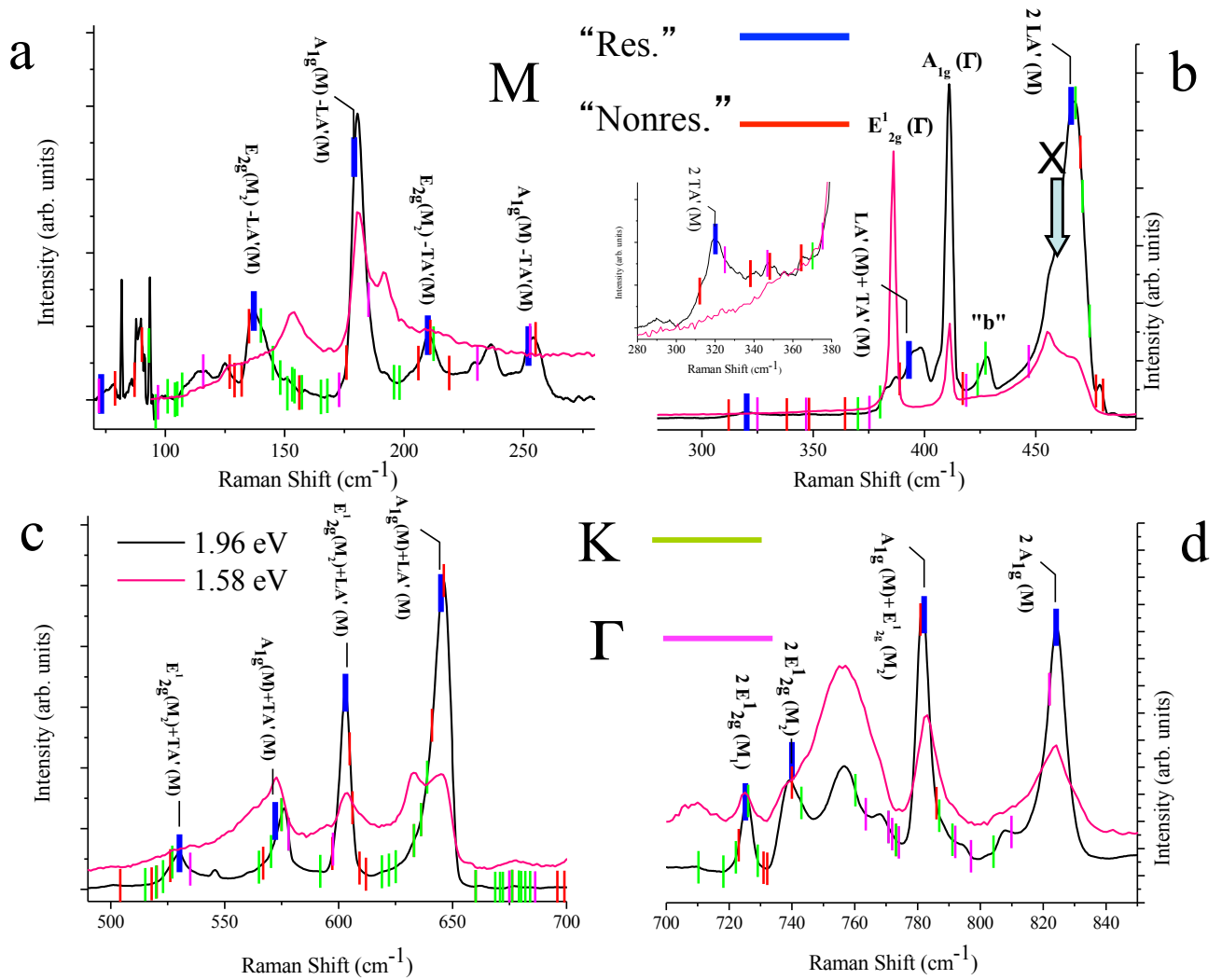


Figure 1 The resonant Raman spectrum of $2H\text{-MoS}_2$ at 95 K measured using excitation energy of 1.96 eV, divided for clarity into four spectral sub-ranges (a-d). Positions of the second-order transitions' bands of origin from M ('Res'-blue, 'Nonres'-red), K (green) and Γ (magenta) Brillouin zone points, that are active under back scattering configuration, are also denoted. For comparison the room temperature Raman spectrum using excitation energy of 1.58 eV is also shown (pink). Note that for the band at $\sim 456\text{ cm}^{-1}$, there is no possible assignment that may point to its origin.

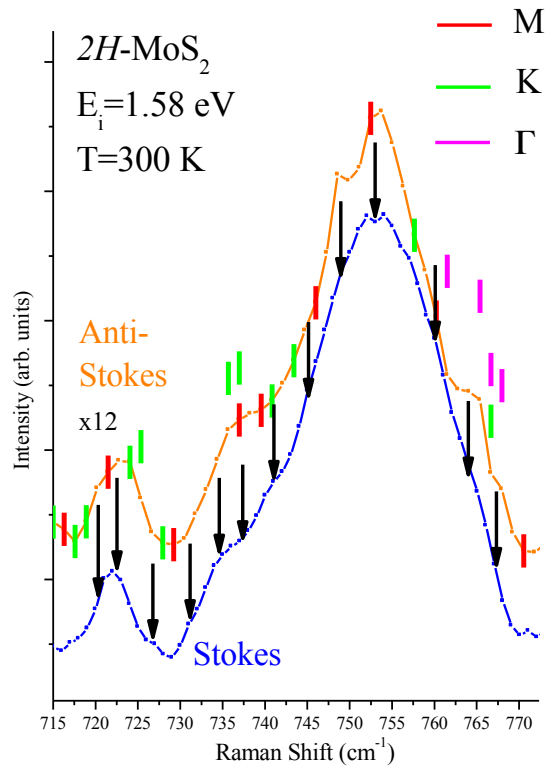


Figure 2 A focus on the spectral profile around the band at $\sim 756\text{ cm}^{-1}$ measured with $E_i=1.58\text{ eV}$ and 300 K . In order to facilitate the differentiation of the large number of potential spectral contributions we show Stokes and anti-Stokes spectra (shown in absolute frequency and scaled to similar intensities). Black arrows point to the central frequencies of the contributing bands. The calculated frequencies of second-order transition (including those attributed in Table 3 to have E_{1g} symmetry) at M, K and Γ points are also shown with the denoted respective colors.

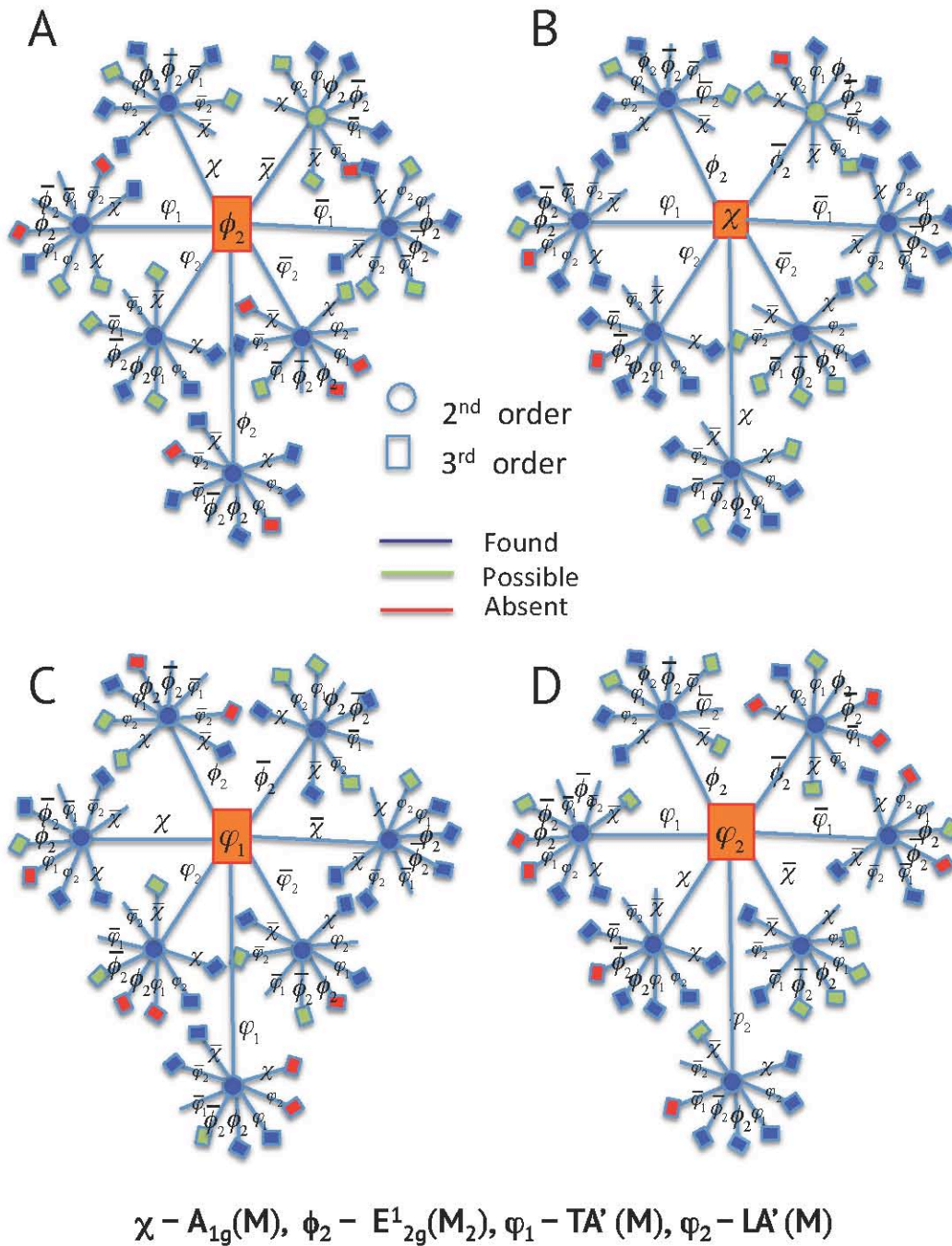


Figure 3 Sequences of all possible contributions (combination and difference bands) are shown in the form of ‘flowers’ for all the 2nd (circles) and 3rd (squares) order resonant transitions from the $E_{2g}(M_2)(\phi_2)$ (A), $A_{1g}(\chi)$ (B) and $TA'(M)$ (φ_1) (C), $LA'(M)$ (φ_2) (D), phonons. Blue represents bands that are detected and red denotes bands that are not detected. Green represents a band that is possibly distinguishable or a band that although not found, we believe one that may possibly be observed under adequately sensitive experimental conditions.

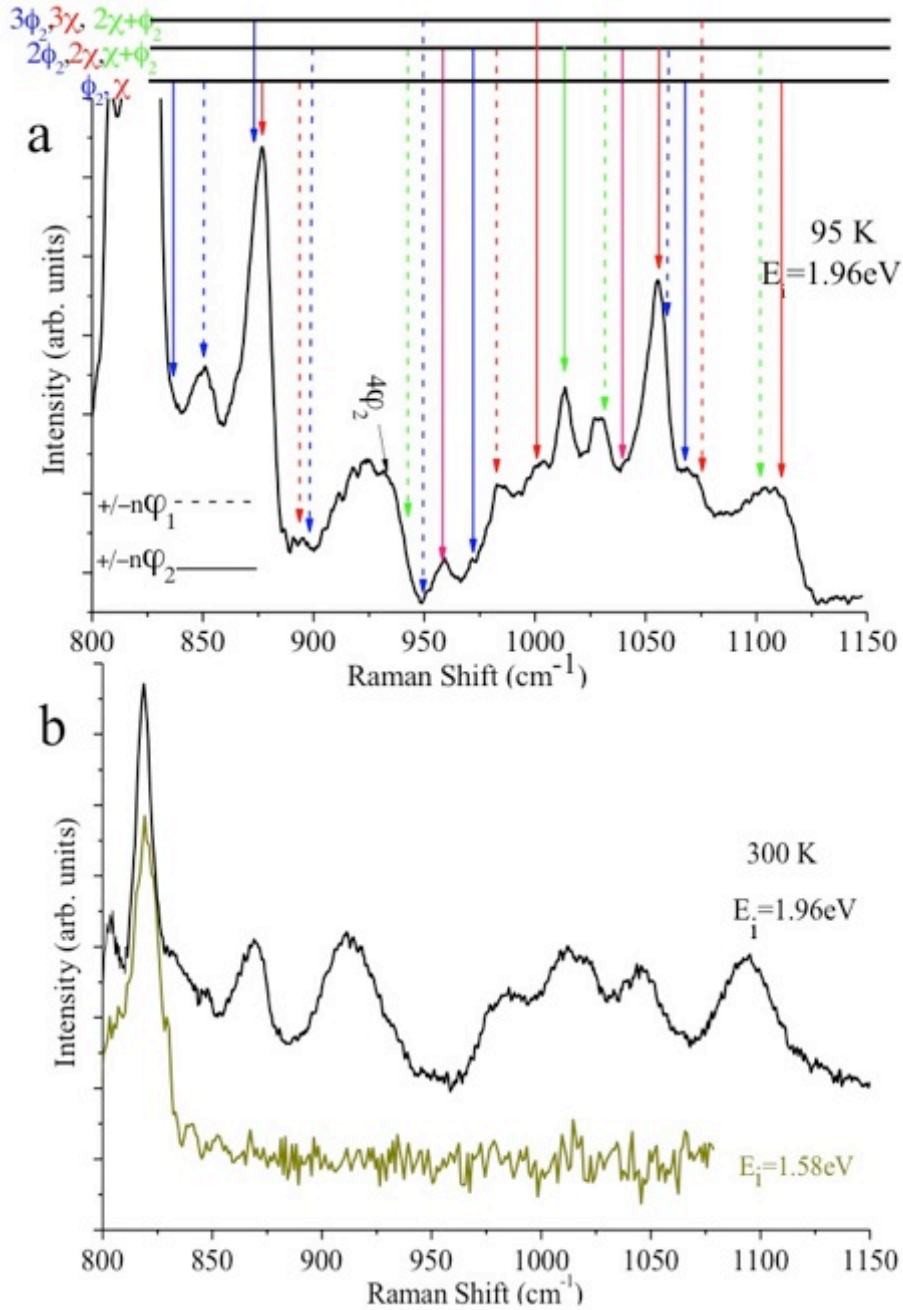


Figure 4 a) A full set of up to 4th order contributions in the range of 830 -1130 cm^{-1} for $E_i = 1.96 \text{ eV}$ at 95 K. The bands are constructed from up to 3rd order combinations of $E_{2g}^1(M_2)(\varphi_2)$ (blue) and $A_{1g}(M)(\chi)$ (red) phonons subtracted or added to TA' (M) (φ_1) (dashed line) or LA' (M) (φ_2) (solid line) phonons. Combinations of $E_{2g}^1(M_2) + A_{1g}(M)$ are shown in green. b) A comparison of Raman spectra at 300 K for $E_i = 1.96 \text{ eV}$ and $E_i = 1.58 \text{ eV}$.

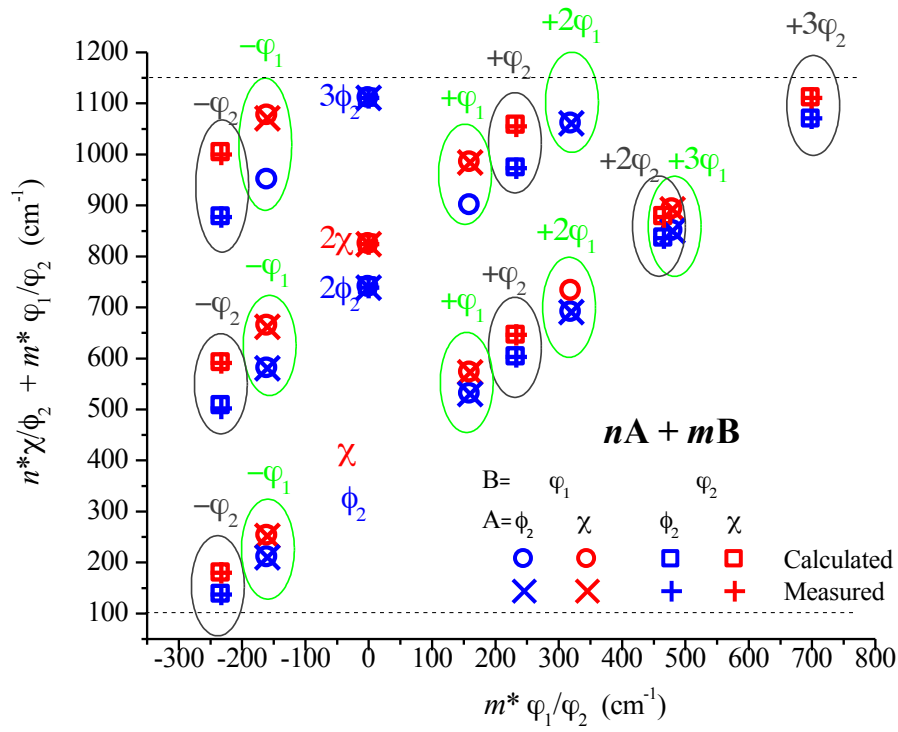


Figure 5 A plot of $nA + mB$ vs. mB ($n = 0-3$, $A = \chi, \varphi_2$, $m = -1, 0, 1, 2, 3$, $B = \varphi_1, \varphi_2$) for various n of the calculated and the measured frequencies.

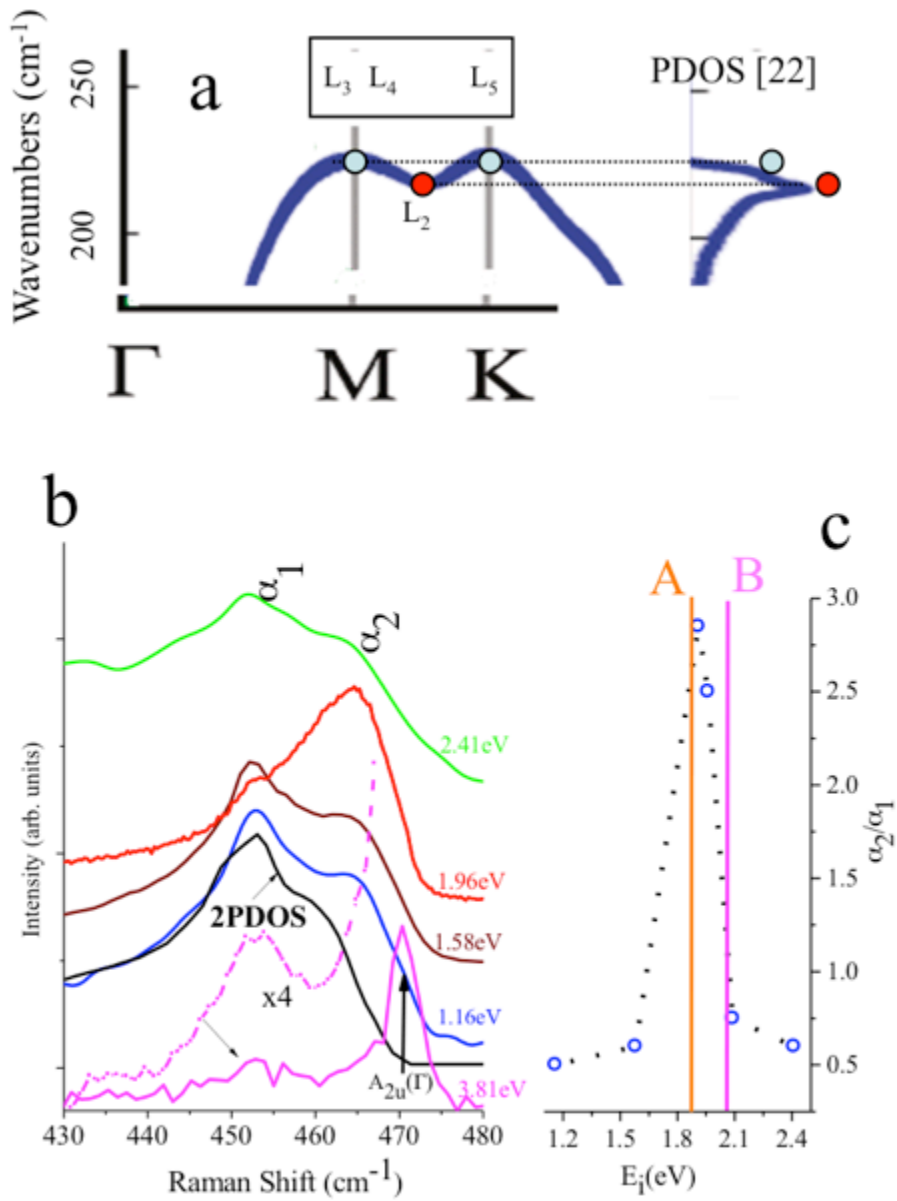


Figure 6 a) The phonon branches in the vicinity of M and K points, calculated by Acata *et al.* [22], with the respective extracted phonon density of states (PDOS) of $2H$ - MoS_2 . b) A comparison of the spectra around $\sim 460 \text{ cm}^{-1}$ for various excitation energies E_i from 1.16 eV to 3.81 eV (dashed dotted line - a zoom of the smoothed lower band). The 2PDOS profile [22] is shown in black line. c) The (α_1/α_2) intensity ratio is depicted for the set of measurements after adding the respective ratios for 1.16, 1.58, 1.91 (taken from [13]), 1.96, 2.09 eV (taken from [6]) and 2.41 eV. The room temperature energies of the A and B excitons are also denoted.

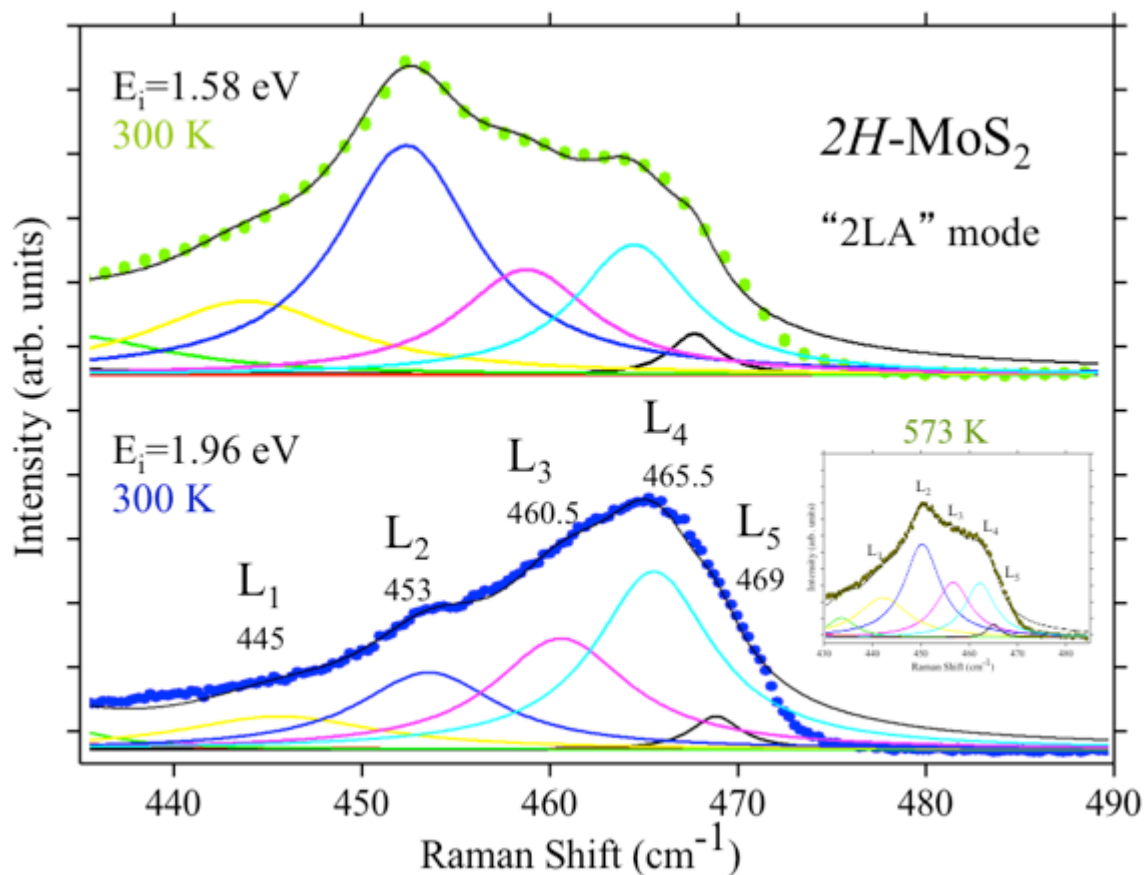


Figure 7 Lorentzian line fit analysis of the $2H\text{-MoS}_2 \sim 460\text{ cm}^{-1}$ band measured at room temperature at $E_i = 1.58\text{ eV}$ (top) and $E_i = 1.96\text{ eV}$ (bottom). It is evident that the spectra are comprised of at least five contributions [31], denoted in the figure as L_1 - L_5 . In the inset of the bottom spectrum shown the spectrum for 573 K with $E_i = 1.96\text{ eV}$. The resemblance of the spectral profile to that of the top spectrum, taken at non-resonant conditions, is evident.

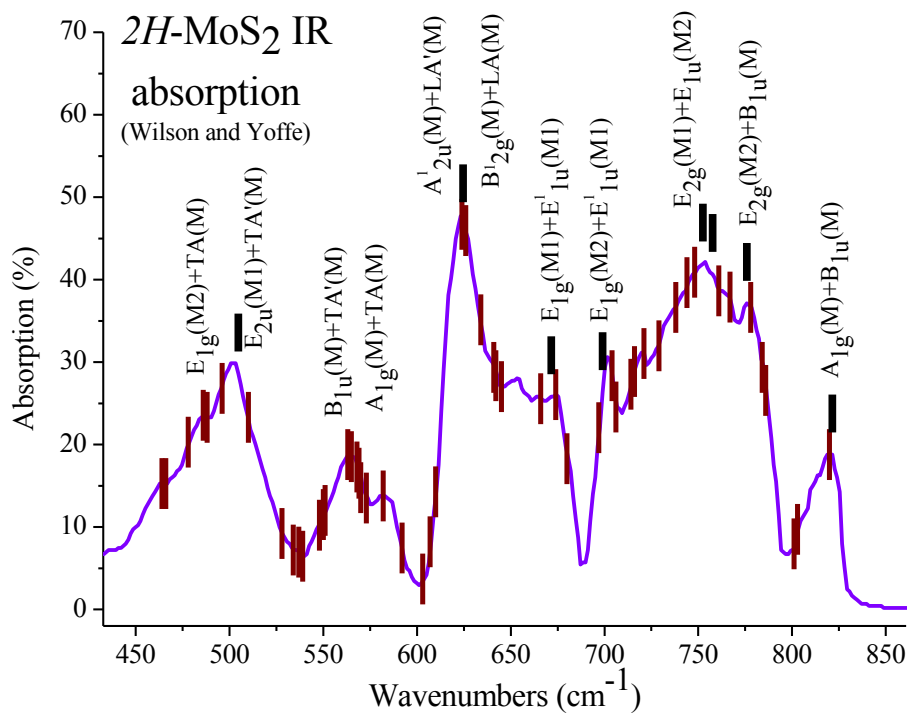


Figure 8 a) The IR absorption spectrum from a 180 μm layer of $2H\text{-MoS}_2$ adapted from Willson and Yoffe [18] with the denoted M point IR allowed combinations presented in Table 3. In black stripes, the absorption bands from Agnihorti [32] are indicated after subtracting from them 5 cm^{-1} in order to take into account temperature effects (as they were measured in 77 K). Attached are proposed assignments to some of the bands. K point second-order potential contributors are not included.

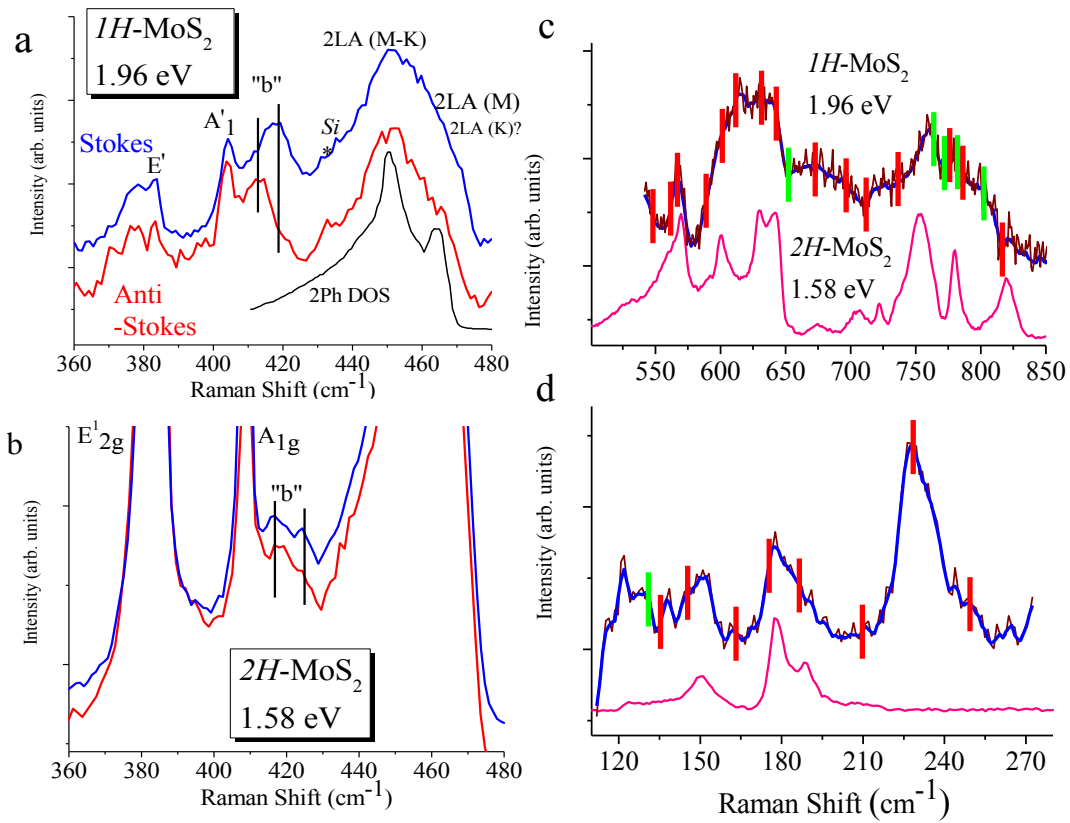


Figure 9 a) The Stokes (blue) and Anti-Stokes (red) Raman spectrum of single layer measured at 300K and E_i of 1.96 eV (shown in absolute frequency and scaled to similar intensities). The spectrum of the ‘2LA band’ is compared to the 2PDOS of single layer calculated by Ataca *et al.* [22]. The $\sim 5 \text{ cm}^{-1}$ shift between the ‘b bands’ of the two branches (similarly to the bulk $2H$ case) are shown. b) Stokes (blue) and Anti-Stokes (red) Raman spectrum of bulk (shown in absolute frequency and scaled to similar intensities), measured at 300 K and E_i of 1.58 eV. Multiphonon spectra for the monolayer in the range of (c) $500\text{-}850 \text{ cm}^{-1}$ and (d) $110\text{-}280 \text{ cm}^{-1}$ are compared with that of 1.58 eV bulk $2H$ spectra. Expected positions of the multiphonon A_1' (M), E' (M_1), LA(M) (red) and Γ point (green) are also shown.

Supporting Information

S1. Reduction of second-order representations and compatibility relations

Compatibility relations relate the basis functions (wave functions) in going from one wave vector to another belonging to a different symmetry group [1]. Such a situation, for example, occurs in *2H*-MoS₂ when going from $\mathbf{k} = 0$ (Γ point with D_{6h} symmetry) to an interior \mathbf{k} point such as the M Brillouin zone point with D_{2h} symmetry or the K Brillouin zone point with D_{3h} symmetry. In order to construct Table 2 we first reduced the representation of all the $M_i \times M_j$ ($i, j=8$) and $K_i \times K_j$ ($i, j=6$) second-order processes into its irreducible constituents and then construct compatibility tables [2, 3] for $\Gamma \xrightarrow{\Sigma} M$ and $\Gamma \xrightarrow{\Lambda} K$. The results of the reduction process are shown in **Tables S1** and **S2** for M and K points, respectively, and the compatibility relations are shown in **Tables S3** and **S4** for M and K points, respectively. For completeness of presentation and further analysis we also show the compatibility table for and $M \xrightarrow{T} K$ in **Table S5**.

After relating the compatibility relations with the reduction process we show in **Tables S6** and **S7** the correlation of M and K points with the Γ point and denote the Raman allowed representations in bold. Let us explore, for example, the $A_g \times A_g$ and $A_u \times A_g$ processes in Table S1. In the former, $A_{1g}(\Gamma) + E_{2g}(\Gamma)$ comes from the D_{6h} point group at Γ and no additional representation originates from $A_g(M) + B_{1g}(M)$ (see Table S6). This gives a total of $A_{1g}(\Gamma) + E_{2g}(\Gamma)$. For $A_u \times A_g$ none of the symmetries contribute and therefore it is not Raman-active. The contribution of $A_{2u}(\Gamma)$ indicates that it does have IR activity.

The same arguments apply to *1H*-MoS₂ for which the results of the reduction process are shown in **Tables S8**.

S2. Some important aspects relating the construction of Table 1

Sourisseau *et al.* presented the calculated phonon dispersion of $2H\text{-MoS}_2$ and phonon symmetries at the M and K points [4]. Recently, more detailed calculated dispersion curves were also published (for example [5]) without specifying the phonon symmetries at the M and K points. The starting point in our analysis (Table 1) is the phonon symmetries assigned in Ref. 4. However, detailed examination of recent calculated dispersion curves (see Fig. 2 of Ref. 5) points to the need to reconsider at least some of the assignments. For example, it seems that some pairs of singly degenerate M point phonons, which remain singly degenerate in Ref. 4, join at the K point to form doubly degenerate phonons. Therefore, we looked at each of those ‘suspected’ pairs with the aid of the compatibility relations along $\Gamma \xrightarrow{\Sigma} M$, $\Gamma \xrightarrow{\Lambda} K$ and $M \xrightarrow{T} K$, which are shown below in Tables S3-S5.

Let us explore, as an example, the ZA and ZA’ phonons, which are singly degenerate at M, but seem in the calculations [5] to joint at the K point into a doubly degenerate phonon. The ZA mode starts at Γ with A_{2u} representation (Table 1) and reaches the M point with either B_{1u} or B_{2g} (Table S3) representations (according to Ref. 4, which maintains similar inversion symmetry at Γ and M, it is the former). The ZA’ mode starts at Γ with B_{2g} representation and reaches the M point with either A_u or B_{3g} representations (according to Ref. 4 it is the latter). Let us now explore (Table S5) the branch of those phonons from M to K ($M \xrightarrow{T} K$ [3]). The ZA phonon should reach the K point with either A_2' or A_1'' representations or will combine with another phonon to construct a doubly degenerate E'' phonon at K. The ZA’ should also reach the K point with either A_2' or A_1'' or will combine with another phonon to construct an E'' phonon. Hence, one can construct the following combinations that may lead to ZA and ZA’ to combine at K into a doubly degenerate phonons: $(B_{1u}(ZA)+A_u(ZA'))$ and $(B_{2g}(ZA)+B_{3g}(ZA'))$. For this to occur the assignment of one of the bands should be altered from that of Ref. 4.

In order to have a more solid interpretation we need now to explore the compatibility relations of $\Gamma \xrightarrow{\Lambda} K$ (Table S4): The ZA should lead to A_2' or combine with another singly degenerate A_1'' phonon to construct an E'' phonon at K. The ZA’ should also lead to A_2' or combine with another singly degenerate A_1'' phonon to construct an E'' phonon at K.

Since both ZA and ZA' are of A_2' representation at the K the scenario of their joining together to form an E'' phonon at the K point is not feasible according to Table S4, since for the E'' phonon the irreducible representation contains $\Lambda_3 + \Lambda_2$ (and not $2\Lambda_3$). We therefore argue that singly degenerate $ZA(M)$ and $ZA'(M)$ should evolve into singly degenerate $ZA(K)$ and $ZA'(K)$ with what seems to be [5] very similar frequencies.

After analyzing all the single degenerate phonons at M that may seem to combine into doubly degenerate phonons at K we argue that there may potentially be only two doubly degenerate phonons at K that will be described in the following.

Each of the doubly degenerate modes at the Γ Brillouin zone point generates two phonon branches that reach the M point with single degenerate representations at two different frequencies [3, 4]. From examining the calculated dispersion curves [5] it seems that for the $E_{2g}^1(\Gamma)$ & $E_{1u}(\Gamma)$ Davydov doublet the frequencies of $E_{2g}^1(M_1)$ and $E_{1u}(M_2)$ are ~ 8 cm^{-1} higher than that of $E_{2g}^1(M_2)$ and $E_{1u}(M_1)$ and for the $E_{1g}(\Gamma)$ & $E_{2u}(\Gamma)$ doublet the frequencies of $E_{1g}(M_1)$ and $E_{2u}(M_1)$ are ~ 24 and ~ 33 cm^{-1} higher than that of $E_{1g}(M_2)$ and $E_{2u}(M_2)$, respectively. While for the latter, the shifts between the two branches were approximated correctly in Ref. 4, for the former it was strongly underestimated with respect to Ref. 5.

We shall explore below the possibility of the construction of doubly degenerate phonon at K from combinations of $E_{1g}(M_1) + E_{2u}(M_1)$ and $E_{2g}^1(M_2) + E_{1u}(M_1)$ phonons. From Table S4 we see that each phonon at M can have one of two representations; even (g) or odd (u) with respect to inversion. Since, as pointed before, according to Ref. 4 all the phonons at M have the same parity to those of their original phonons at Γ , it is evident from Table S5 that in order for the above scenario to apply the representation of one of the phonons at M of Ref. 4 needs to be altered.

For example, there are two possibilities for $E_{2g}^1(M_1)$ to form with $E_{1u}(M_2)$ a phonon with E' representation at K (and denoted in Table 1 as $E_{ug}(K_2)$): $B_{1g}+A_g$ and $B_{3u}+B_{2u}$. In the first case the representation of the $E_{1u}(M_2)$ phonon will be altered from B_{3u} to A_g and in the second case the representation of the $E_{2g}^1(M_1)$ phonon will be altered from B_{1g} to B_{3u} . In our analysis we selected the second option. The reason for this selection is that the $2E_{2g}^1(M_1)$ band at 725 cm^{-1} , which is Raman allowed at all representations, behaves resonantly (also with respect to temperature dependence, not shown here) but

combinations like $E_{2g}^1(M_1) + A_{1g}(M)$ (at 774 cm^{-1}) and particularly $E_{2g}^1(M_1) + E_{2g}^1(M_2)$ (at 732 cm^{-1}) are definitely absent. We tentatively used this observation as a support for the attribution of the representation of the $E_{2g}^1(M_1)$ phonon to be odd with respect to inversion, with B_{3u} representation rather than B_{1g} (as assigned in Ref. 4). However, since combination bands of $2E_{2g}^1(M_1)$ with all the ‘resonant group’ phonons are allowed, evidence to their appearance may be found in the spectra. In fact, some of the proposed Raman transition energies in Table 5 may be alternatively assigned to the following combinations with $2E_{2g}^1(M_1)$ (ϕ_1^2): $312 - \phi_1^2\bar{\chi}$, $356 - \phi_1^2\bar{\phi}_2$, $566 - \bar{\varphi}_1\phi_1^2$, $958 - \varphi_2\phi_1^2$, $1043 - \varphi_1^2\phi_1^2$, $1117 - \varphi_1\varphi_2\phi_1^2$ (see Table 1 for the various notations)

Finally, it noteworthy that if we would have selected $E_{1u}(M_2)$ phonon to be altered from B_{3u} to A_g the activity and polarization dependent properties of the second-order transitions of the $E_{1u}(M_2)$ and $E_{2g}^1(M_1)$ phonons, as expressed in Table 3, would have been modified. Therefore, with all the ‘tools’ provided in this paper, Table 3 may be revisited if new theoretical evidence with regard to the symmetry assignments of the Brillouin edge phonons will become available. Similar rationale to the construction of $E_{ug}(K_2)$ applies to the construction of $E_{ug}(K_1)$, which originates from $E_{1g}(M_1)$ and $E_{2u}(M_2)$.

The same procedure that was described above for bulk $2H$ -MoS₂ was applied to the construction of Tables 6-8 for the monolayer $1H$ -MoS₂. The compatibility relations and the correlation of M point with the Γ point representations, are shown in **Table S9** and **S10**, respectively.

References

1. M.S. Dresselhaus, G. Dresselhaus, A. Jorio, ”*Group theory, Application to the Physics of Condensed Matter*” (Springer, Berlin 2008) p. 209
2. D.L. Rousseau, R.P. Bauman, S.P.S. Porto *J. Raman Spectrosc.*, 10, 253 (1981)
3. Aroyo M.I., A. Kirov, C. Capillas, J. M. Perez-Mato & H. Wondratschek, *Acta Cryst.* A62 115 (2006); <http://www.cryst.ehu.es>.
4. C. Sourisseau, F. Cruege, and M. Fouassier, *Chem. Phys.* 150, 281 (1991)
5. A. Molina-Sánchez and L. Wirtz *Phys. Rev. B* 84, 155413 (2011)

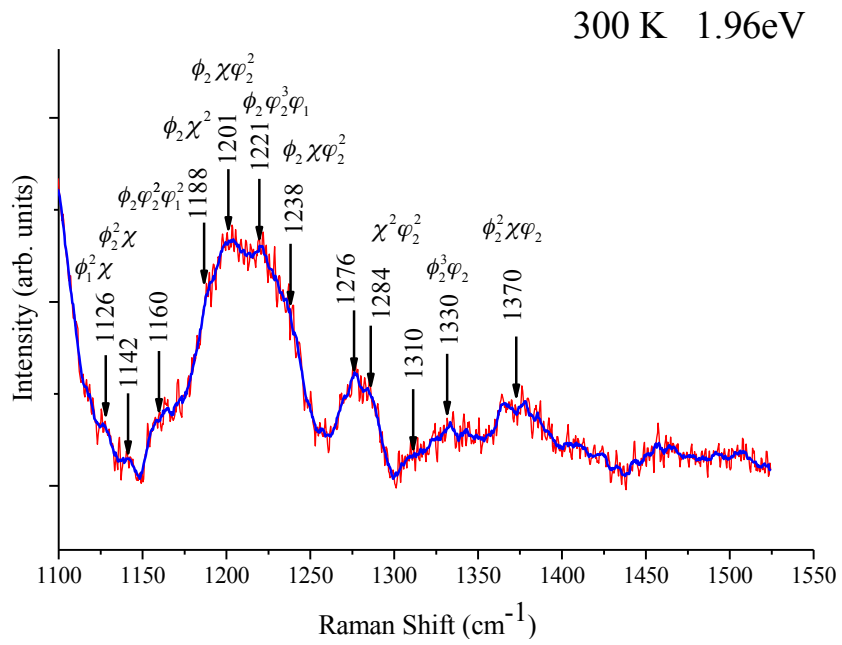


Figure S1 The ‘high end’ of the $2H$ - MoS_2 Raman spectrum, measured at 300 K for $E_i = 1.96$ eV. Assignments of up to 5th order transitions are proposed. For phonons notations see Table 1.

Table S1 The reduction of the $M_i \times M_j$ ($i, j=8$) second-order representations to the irreducible representations in $2H\text{-MoS}_2$. The representations for Γ are denoted in blue and the representation for M are denoted in black.

M/D _{2h}	A _g	A _u	B _{1g}	B _{1u}	B _{2g}	B _{2u}	B _{3g}	B _{3u}
A _g	$A_{1g}+E_{2g}$ +A _g +B _{1g}	$A_{1u}+E_{2u}$ +A _u +B _{1u}	$A_{2g}+E_{2g}$ +A _g +B _{1g}	$A_{2u}+E_{2u}$ +A _u +B _{1u}	$B_{1g}+E_{1g}^+$ B _{2g} +B _{3g}	$B_{1u}+E_{1u}^+$ B _{2u} +B _{3u}	$B_{2g}+E_{1g}^+$ B _{2g} +B _{3g}	$B_{2u}+E_{1u}^+$ B _{2u} +B _{3u}
A _u		$A_{1g}+E_{2g}$ +A _g +B _{1g}	$A_{2u}+E_{2u}$ +A _u +B _{1u}	$A_{2g}+E_{2g}$ +A _g +B _{1g}	$B_{1u}+E_{1u}^+$ B _{2u} +B _{3u}	$B_{1g}+E_{1g}^+$ B _{2g} +B _{3g}	$B_{2u}+E_{1u}^+$ B _{2u} +B _{3u}	$B_{2g}+E_{1g}^+$ B _{2g} +B _{3g}
B _{1g}			$A_{1g}+E_{2g}$ +A _g +B _{1g}	$A_{1u}+E_{2u}$ +A _u +B _{1u}	$B_{2g}+E_{1g}^+$ B _{2g} +B _{3g}	$B_{2u}+E_{1u}^+$ B _{2u} +B _{3u}	$B_{1g}+E_{1g}^+$ B _{2g} +B _{3g}	$B_{1u}+E_{1u}^+$ B _{2u} +B _{3u}
B _{1u}				$A_{1g}+E_{2g}$ +A _g +B _{1g}	$B_{2u}+E_{1u}^+$ B _{2u} +B _{3u}	$B_{2g}+E_{1g}^+$ B _{2g} +B _{3g}	$B_{1u}+E_{1u}^+$ B _{2u} +B _{3u}	$B_{1g}+E_{1g}^+$ B _{2g} +B _{3g}
B _{2g}					$A_{1g}+E_{2g}^+$ A _g +B _{1g}	$A_{1u}+E_{2u}^+$ A _u +B _{1u}	$A_{2g}+E_{2g}^+$ A _g +B _{1g}	$A_{2u}+E_{2u}^+$ A _u +B _{1u}
B _{2u}						$A_{1g}+E_{2g}^+$ A _g +B _{1g}	$A_{2u}+E_{2u}^+$ A _u +B _{1u}	$A_{2g}+E_{2g}^+$ A _g +B _{1g}
B _{3g}							$A_{1g}+E_{2g}^+$ A _g +B _{1g}	$A_{1u}+E_{2u}^+$ A _u +B _{1u}
B _{3u}								$A_{1g}+E_{2g}^+$ A _g +B _{1g}

Table S2 The reduction of the $K_i \times K_j$ ($i, j=6$) second-order representations to the irreducible representations in $2H\text{-MoS}_2$. The representation for Γ are denoted in blue and the representation for K in black.

K/D _{3h}	A ₁	A ₁ ^{''}	A ₂	A ₂ ^{''}	E	E ^{''}
A ₁	$A_{1g}+B_{1u}$ +A ₁	$A_{2g}+B_{2u}$ +A ₁ ^{''}	$A_{1u}+B_{1g}$ +A ₂	$A_{2u}+B_{2g}$ +A ₂ ^{''}	$E_{2g}+E_{1u}$ +E	$E_{2u}+E_{1g}$ +E ^{''}
A ₁ ^{''}		$A_{1g}+B_{1u}$ +A ₁	$A_{2u}+B_{2g}$ +A ₂ ^{''}	$A_{1u}+B_{1g}$ +A ₂	$E_{2g}+E_{1u}$ +E	$E_{2u}+E_{1g}$ +E ^{''}
A ₂			$A_{1g}+B_{1u}$ +A ₁	$A_{2g}+B_{2u}$ +A ₁ ^{''}	$E_{2u}+E_{1g}$ +E	$E_{2g}+E_{1u}$ +E
A ₂ ^{''}				$A_{1g}+B_{1u}$ +A ₁	$E_{2u}+E_{1g}$ +E	$E_{2g}+E_{1u}$ +E
E					$A_{1g}+A_{2g}+B_{1u}$ +B _{2u} +E _{2g} +E _{1u} +A ₁ +A ₁ ^{''} +E	$A_{1u}+A_{2u}+B_{1g}$ +B _{2g} +E _{2u} +E _{1g} ^{''} +A ₂ +A ₂ ^{''} +E
E ^{''}						$A_{1g}+A_{2g}+B_{1u}$ +B _{2u} +E _{2g} +E _{1u} ^{''} +A ₁ +A ₁ ^{''} +E

Table S3 Compatibility relations along Σ in $2H\text{-MoS}_2$

Compatibility relation between M and Σ		Compatibility relation between Γ and Σ	
$D_{2h}(M)$	Irreducible representations	$D_{6h}(\Gamma)$	Irreducible representations
A_g	Σ_1	A_{1g}	Σ_1
A_u	Σ_4	A_{1u}	Σ_4
B_{1g}	Σ_2	A_{2g}	Σ_2
B_{1u}	Σ_3	A_{2u}	Σ_3
B_{2g}	Σ_3	B_{1g}	Σ_3
B_{2u}	Σ_2	B_{1u}	Σ_2
B_{3g}	Σ_4	B_{2g}	Σ_4
B_{3u}	Σ_1	B_{2u}	Σ_1
		E_{1g}	$\Sigma_4 + \Sigma_3$
		E_{1u}	$\Sigma_2 + \Sigma_1$
		E_{2g}	$\Sigma_2 + \Sigma_1$
		E_{2u}	$\Sigma_4 + \Sigma_3$

Table S4 Compatibility relations along Λ in $2H\text{-MoS}_2$

Compatibility relation between K and Λ		Compatibility relation between Γ and Λ	
$D_{3h}(K)$	Irreducible representations	$D_{6h}(\Gamma)$	Irreducible representations
A_1'	Λ_1	A_{1g}	Λ_1
A_1''	Λ_2	A_{1u}	Λ_2
A_2'	Λ_3	A_{2g}	Λ_4
A_2''	Λ_4	A_{2u}	Λ_3
E'	$\Lambda_4 + \Lambda_1$	B_{1g}	Λ_2
E''	$\Lambda_3 + \Lambda_2$	B_{1u}	Λ_1
		B_{2g}	Λ_3
		B_{2u}	Λ_4
		E_{1g}	$\Lambda_3 + \Lambda_2$
		E_{1u}	$\Lambda_4 + \Lambda_1$
		E_{2g}	$\Lambda_4 + \Lambda_1$
		E_{2u}	$\Lambda_3 + \Lambda_2$

Table S5 Compatibility relations along T in 2H-MoS₂

Compatibility relation between K and T		Compatibility relation between M and T	
D _{3h} (K)	Irreducible representations	D _{2h} (M)	Irreducible representations
A ₁ '	T ₁	A _g	T ₁
A ₁ ''	T ₂	A _u	T ₂
A ₂ '	T ₃	B _{1g}	T ₄
A ₂ ''	T ₄	B _{1u}	T ₃
E'	T ₁ + T ₄	B _{2g}	T ₂
E''	T ₂ + T ₃	B _{2u}	T ₁
		B _{3g}	T ₃
		B _{3u}	T ₄

Table S6 The correlation of the M point representations with the Γ point in 2H-MoS₂

$A_g(M) = A_{1g}(\Gamma) + E_{2g}(\Gamma)$
$A_u(M) = A_{1u}(\Gamma) + E_{2u}(\Gamma)$
$B_{1g}(M) = A_{2g}(\Gamma) + E_{2g}(\Gamma)$
$B_{1u}(M) = A_{2u}(\Gamma) + E_{2u}(\Gamma)$
$B_{2g}(M) = B_{1g}(\Gamma) + E_{1g}(\Gamma)$
$B_{2u}(M) = B_{1u}(\Gamma) + E_{1u}(\Gamma)$
$B_{3g}(M) = B_{2g}(\Gamma) + E_{1g}(\Gamma)$
$B_{3u}(M) = B_{2u}(\Gamma) + E_{1u}(\Gamma)$

Table S7 The correlation of the K point representations with the Γ point in 2H-MoS₂

$A_1'(K) = A_{1g}(\Gamma) + B_{1u}(\Gamma) + E_{2g}(\Gamma) + E_{1u}(\Gamma)$
$A_1''(K) = A_{1u}(\Gamma) + B_{1g}(\Gamma) + E_{1g}(\Gamma) + E_{2u}(\Gamma)$
$A_2'(K) = A_{2u}(\Gamma) + B_{2g}(\Gamma) + E_{1g}(\Gamma) + E_{2u}(\Gamma)$
$A_2''(K) = A_{2g}(\Gamma) + B_{2u}(\Gamma) + E_{2g}(\Gamma) + E_{1u}(\Gamma)$
$E'(K) = E_{2g}(\Gamma) + E_{1u}(\Gamma)$
$E''(K) = E_{2u}(\Gamma) + E_{1g}(\Gamma)$

Table S8 The reduction of the $M_i \times M_j$ ($i, j=4$) second-order representations to the irreducible representations in $IH\text{-MoS}_2$. The representations for Γ are denoted in blue and the representation for M are denoted in black.

M/C_{2v}	A_1	A_2	B_1	B_2
A_1	$A_1'+E'$ + A_1+B_1	$A_1''+E''$ + A_2+B_2	$A_2'+E'$ + A_1+B_1	$A_2''+E''$ + A_2+B_2
A_2		$A_1'+E'$ + A_1+B_1	$A_2''+E''$ + A_2+B_2	$A_2'+E'$ + A_1+B_1
B_1			$A_1'+E'$ + A_1+B_1	$A_1''+E''$ + A_2+B_2
B_2				$A_1'+E'$ + A_1+B_1

Table S9 Compatibility relations along Σ in $IH\text{-MoS}_2$

Compatibility relation between M and Σ		Compatibility relation between Γ and Σ	
$C_{2v}(M)$	Irreducible representations	$D_{3h}(\Gamma)$	Irreducible representations
A_1	Σ_1	A_1'	Σ_1
A_2	Σ_3	A_1''	Σ_3
B_1	Σ_4	A_2'	Σ_2
B_2	Σ_2	A_2''	Σ_4
		E'	$\Sigma_2 + \Sigma_1$
		E''	$\Sigma_4 + \Sigma_3$

Table S10 The correlation of the M point representations with the Γ point in $IH\text{-MoS}_2$

$A_1(M) = A_1'(\Gamma) + E'(\Gamma)$
$A_2(M) = A_1''(\Gamma) + E''(\Gamma)$
$B_1(M) = A_2''(\Gamma) + E''(\Gamma)$
$B_2(M) = A_2'(\Gamma) + E'(\Gamma)$